STUDY OF REACTION MECHANISM IN P+^{51}V AND P+^{209}Bi SYSTEMS AT VARIOUS PROTON ENERGIES

A thesis submitted to the School of Graduate Studies

Addis Ababa University

IN PARTIAL FULFILLMENT OF THE REQUIREMENTS FOR THE DEGREE OF MASTER OF SCIENCE IN PHYSICS

By

DESSIE MELESE

Addis Ababa, Ethiopia

June, 2016

ADDIS ABABA UNIVERSITY

DEPARTMENT OF

PHYSICS

Advisor: _____

Prof. A. K. Chaubey

Examiner: _____

Dr. Tilahun Tesfaye

Examiner: _____

Dr. S. Bhatnagar

ADDIS ABABA UNIVERSITY

Date: 16/06/2016

Author: **Dessie Melese**

Title: **Study of Reaction Mechanisms in P+^{51}V and P+^{209}Bi Systems at Various Proton Energies**

Department: **Physics**

Degree: **M.Sc.** Convocation: **June** Year: **2016**

Table of Contents

TABLE OF CONTENTS I
LIST OF FIGURES I
ABSTRACT III
ACKNOWLEDGEMENTS IV
1. INTRODUCTION 1
2. THEORIES OF NUCLEAR REACTION 3
2.1. ENERGETICS OF NUCLEAR REACTIONS 3
2.2. PARTIAL WAVE ANALYSIS OF REACTION OF CROSS-SECTION 4
2.3. MECHANISMS OF NUCLEAR REACTION 8
2.3.1. COMPOUND NUCLEUS REACTION MECHANISM 9
2.3.2. DIRECT REACTION MECHANISM 17
2.3.3. THE EXCITON MODEL 18
3. THE COMPUTER CODES 20
3.1. THE COMPLET CODE 20
3.2. DESCRIPTION OF INPUT PARAMETERS 21
4. EXPERIMENTAL MEASUREMENT TECHNIQUES OF EXCITATION FUNCTIONS 26
4.1. ACTIVATION CROSS-SECTION 26
4.2. EXPERIMENTAL RESULTS 28
5. CALCULATIONS OF EXCITATION FUNCTIONS FOR SOME ^{51}V(P,XN) AND ^{209}Bi(P,XN) REACTIONS 29
5.1. COMPARING INPUT PARAMETERS 29
5.1.1. EFFECT OF PLD ON EXCITATION FUNCTION 29
5.1.2. EFFECTS OF CMFP VALUES ON PE EXCITATION FUNCTIONS 35
5.2. COMPARING CALCULATED AND MEASURED CROSS-SECTIONS 39
5.2.1. EXCITATION FUNCTIONS OF (P,N) REACTIONS 40
5.2.2. COMPARISON ON EXCITATION FUNCTIONS OF (P,3N) REACTIONS 44
5.2.3. EXCITATION FUNCTIONS OF (P,4N) REACTIONS 46
5.2.4. CONFIRMATION OF ABSENCE OF EQ DECAY IN SOME REACTIONS 48
5.3. CONCLUSION 50
REFERENCES 51

List of Figures

FIGURE 2.1: REPRESENTATION OF IMPACT PARAMETER ON A TARGET NUCLEUS. 5

FIGURE 2.2: VARIATION OF REACTION CROSS-SECTION WITH PROJECTILE ENERGY. 6

FIGURE 2.3: NEAR THRESHOLD BEHAVIOR OF NEUTRON AND CHARGED PARTICLE INDUCED REACTIONS . 7

FIGURE 2.4: NEUTRON EMISSION SPECTRUM FOR DIFFERENT NUCLEAR REACTION MECHANISMS. 8

FIGURE 2.5: GHOSHAL EXPERIMENTAL VERIFICATION OF BOHR'S THEORY . 12

FIGURE 2.6: SPECTRUM OF EVAPORATED NEUTRONS. 15

FIGURE 2.7: EXCITATION FUNCTION FOR THE ^{209}BI(A,XN) REACTIONS. 16

FIGURE 2.8: REPRESENTATION OF THE EQUILIBRATION PROCESS AS FORMULATED IN THE EXCITON MODEL. 18

FIGURE 5.1: COMPARING PLD VALUES FOR PRE-COMPOUND REACTION OF ^{51}V(P,N). 30

FIGURE 5.2: COMPARING PLD FOR EQUILIBRIUM DECAY OF ^{51}V(P,N) . 31

FIGURE 5.4: EFFECTS OF PLD ON PRE-COMPOUND CROSS-SECTIONS ^{51}V(P,4N) . 32

FIGURE 5.3: EFFECTS OF PLD ON PRE-COMPOUND EXCITATION FUNCTION OF ^{51}V(P,3N) 32

FIGURE 5.5: EFFECT OF PLD ON PRE-EQUILIBRIUM CROSS-SECTIONS OF ^{209}BI(P,N) 33

FIGURE 5.6: EFFECT OF PLD ON EQUILIBRIUM EXCITATION FUNCTION OF ^{209}BI(P,N) 33

FIGURE 5.7: EFFECT OF PLD ON EQUILIBRIUM EXCITATION FUNCTION OF ^{209}BI(P,3N). 34

FIGURE 5.8: EFFECTS OF PLD ON PRE-EQUILIBRIUM EXCITATION FUNCTION OF ^{209}BI(P,4N). 35

FIGURE 5.9: : EFFECT OF CMFP VALUES ON EXCITATION FUNCTIONS OF ^{51}V(P,N) AT A = A_{CN}/9. 36

FIGURE 5.10: EFFECT OF CMFP VALUES ON EXCITATION FUNCTIONS OF ^{51}V(P,3N) AT A = A_{CN}/10 36

FIGURE 5.11: COMPARING CMFP VALUES FOR ^{209}BI(P,N) REACTION, A = $A_{CN}/10$ 37

FIGURE 5.12: COMPARING CMFP VALUES FOR ^{209}BI(P,3N) REACTION , A = $A_{CN}/14$ 38

FIGURE 5.13: COMPARING CMFP VALUES FOR ^{209}BI(P,4N) REACTION, A = $A_{CN}/14$. 39

FIGURE 5.13: COMPARING CMFP VALUES FOR ^{209}BI(P,4N) REACTION, A = $A_{CN}/14$. 39

FIGURE 5.14: EXPERIMENTAL AND THEORETICAL EXCITATION FUNCTIONS FOR ^{51}V(p,n) 41

FIGURE 5.15: EXPERIMENTAL AND THEORETICAL EXCITATION FUNCTIONS FOR ^{209}Bi(p,n). 42

FIGURE 5.16: MEASURED AND CALCULATED EXCITATION FUNCTIONS FOR ^{51}V(P,N) AND ^{209}BI(P,N). 43

FIGURE 5.17: EXPERIMENTAL AND THEORETICAL EXCITATION FUNCTIONS FOR ^{51}V(p,3n) REACTION. 44

FIGURE 5.18: MEASURED AND CALCULATED EXCITATION FUNCTIONS FOR ^{209}Bi(p,3n). 45

FIGURE 5.19: EXPERIMENTAL AND THEORETICAL EXCITATION FUNCTIONS FOR ^{51}V(p,4n) . 47

FIGURE 5.20: EXPERIMENTAL AND THEORETICAL EXCITATION FUNCTIONS FOR ^{209}Bi(p,4n). 48

FIGURE 5.21: PEAK CROSS-SECTION VARIATION WITH PROTON ENERGY FOR ^{209}BI(P,XN) REACTIONS. 49

FIGURE 5.22: PEAK CROSS-SECTION VARIATION WITH PROTON ENERGY FOR ^{51}V(P,XN) REACTIONS. 49

Abstract

In this thesis, proton induced reactions on ^{51}V and ^{209}Bi have been studied for various proton energies (7 - 70 MeV). Theoretical equilibrium (EQ) and pre-equilibrium (PE) excitation functions are compared with experimental values. The study showed that the EQ excitation functions are not comparable to that of the experimental at higher energies in all reactions. It is also observed that neither EQ nor PE excitation functions are compatible to that of the experimental for $^{51}V(p,3n)$ and $^{51}V(p,4n)$ reactions; the cross-section peaks of $^{209}Bi(p,xn)$ reactions increase as the number of emitting neutrons increases from one to three; and the cross-section values of $^{51}V(p,n)$ reaction is higher than that of $p+^{209}Bi$ reaction at proton energies below about 20 MeV.

Based on these observations, conclusions are drawn about the failure of the pure equilibrium reaction in its decay to explain the experimental data in the high energy tail portion of the excitation functions, which, however, are explained by pre-equilibrium theory; about the validity of Bohr's theory that EQ decay takes place at lower energies for the lighter target (^{51}V) and at lower and medium energies for the heavier target (^{209}Bi); and about the presence of higher probability for $^{51}V(p,n)$ reaction to occur compared to that of $p+^{209}Bi$ at proton energies below 20 MeV.

Acknowledgements

First I would like to extend my deepest and sincere gratitude to my advisor Prof. A. K. Chaubey for his enthusiastic guidance, encouragement and unlimited supports during my work and write up phase. I am also very thankful to my colleagues, and other friends, to my family and other people who contributed to the completion of this thesis. Finally, I must express my very profound gratitude to MOE, which sponsored me this full time education and to AAU for providing me different services and facilities such as free internet access throughout my years of study and through the process of writing this thesis.

CHAPTER 1

INTRODUCTION

Two different nucleons may undergo nuclear reaction if they approach each other within a distance of the order of nuclear dimensions (~10^{-15} m). This can be achieved by bombarding stationary *target* nuclei with a beam of projectile nuclei coming from an accelerator or from a radioactive substance. Before the invention of accelerators, nuclear reactions were induced by irradiating targets with α-beam, the only projectile available from radioactive sources initially. It was Rutherford who observed, in 1919, the first nuclear reaction in laboratory using α-particle beam, obtained from the radioisotope bismuth (^{214}Bi). His reaction was

$$\alpha + {}^{14}_{7}N \rightarrow {}^{17}_{8}O + p$$

Accelerated bi-products of a nuclear reaction may also induce further nuclear reactions. However, the bi-products emitted from reactions induced by α-particle projectiles from radioactive sources are too slow to induce nuclear reaction. With the development of accelerators around 1930, the possibilities multiplied by changing the energy of projectile. Unlike projectiles from radioactive sources, projectiles from accelerator machines have high flux, focused beam, and continuous and sufficiently high energy. Accelerators led to the description of the structure of the nuclei and even more specifically the structure of nucleons (proton and neutron). Moreover, modern accelerators are in use in producing radioactive isotope residues that have various uses and applications.

Nuclear reactions, like chemical reactions, can occur via different reaction mechanisms. In general, all the different reaction mechanisms are classified into two categories. These are the compound nucleus reaction mechanism which occurs at lower energies, and the direct reaction mechanism that occurs at higher energies. Bohr's compound nucleus theory, proposed in 1936, has been extremely useful in the correlation and interpretation of nuclear reactions. According to Bohr, the nuclear reaction takes place in two distinct and independent stages: compound nucleus formation, and its decay. During compound nucleus formation, the excitation energy and angular momentum of the projectile are shared thoroughly among the constituting nucleons until the system

reaches to equilibrium. The compound nucleus formed is unstable and decays in to the final products of the nuclear reaction. The formed compound nucleus can live a relatively long time. Sometimes particles are emitted before equilibrium is reached, which is the mechanism of pre-compound nucleus decay. The length of the interaction time of a pre-compound reaction is usually in between those of the two reaction mechanisms.

In direct reactions, the incident particle interacts primarily at the surface of the target nucleus and part of its energy is transferred directly to one or a small group of surface nucleons and it proceeds without compound nucleus formation. The interaction time is very much shorter than that of the corresponding compound nucleus reaction. Because of this, the reaction products exhibit certain characteristics which are entirely different from those observed in compound nucleus reaction.

One of the important quantities of interest for a specific set of kinematic variables for nuclear reaction mechanisms is the reaction cross-section. The nuclear reaction cross-section can be defined in terms of the number of particles emitted, or of nuclei undergoing transmutation for a specified number of incident particles. It has dimension of area and is usually measured in barn (b), where 1 b = 10^{-24} cm^2. The distribution of the reaction cross-section as a function of the incident beam energy is called *excitation function*. The graph of the excitation function enables us to validate nuclear reaction mechanisms by comparing its measured and calculated values for many nucleons.

In the present thesis, theoretical excitation functions or cross-sections are calculated for some ^{51}V(p,xn) and ^{209}Bi(p,xn) reactions using COMPLET computer code. The calculated values are compared with experimental results taken from EXFOR data reference. Based on observations, conclusions are drawn about the failure of the pure equilibrium reaction in its decay to explain the experimental data in the high energy tail portion of the excitation functions, which, however, are explained by pre-equilibrium theory; about validity of Bohr's theory on ^{51}V and ^{209}Bi targets; about independence of excitation functions on PLD and CMFP values at lower proton energies and about the presence of higher probability for ^{51}V(p,n) reaction to occur compared to that of p+^{209}Bi at lower proton energies (< 20 MeV).

CHAPTER 2

THEORIES OF NUCLEAR REACTION

A nuclear reaction occurs if two or more nuclei interact among each other through exchange of energy/momentum or nucleon (or combination of nucleons). Two different nuclei undergo nuclear reaction if they approach each other within a distance of the order of nuclear dimensions (~10^{-15} m). For two nuclides to come closer to one another, one must have sufficient kinetic energy with respect to the other so that it overcomes the barrier potential. A convenient way to induce a nuclear reaction is to bombard stationary target nuclei with a beam of projectile nuclei. During a nuclear reaction, the interacting system may emit outgoing particle(s) and/or radiations, leaving behind a residual nucleus.

$$\text{Projectile} + \text{Target} \rightarrow \text{Residual Nucleus} + \text{Emitted Particle(s)}$$

If an incident particle 'x' induces a nuclear reaction on a target nucleus 'T' and particle 'y' is emitted leaving behind a residual nucleus 'R', then a shorthand way to denote such a reaction is T(x,y)R. One important consequence of nuclear reaction is that total number of nucleons is conserved. That is, the number of nucleons of the reacting system is equal to the number of nucleons of the emitted particles plus number of nucleons of the residual nucleus.

2.1. Energetics of nuclear reactions

The energy released or absorbed in a nuclear reaction is called the *energy balance of the reaction* or simply the *Q-value*, and is defined as the difference in mass energies of the products and the reactants. If the kinetic energy of the projectile 'x' in T(x,y)R reaction is ε, then the energy balance is given by

$$Q = [m_x + m_T - (m_y + m_R)]c^2 = \in_R + \in_y - \varepsilon \qquad 2.1$$

where m's and $\in$'s represent masses and kinetic energies of the particles, respectively. Note that Q is an important quantity for nuclear reactions. If Q is positive, the reaction is *exoergic* while if it is negative, the reaction is *endoergic*. The other idea to be noted is that since 'R' and 'y' may be formed in excited states, their masses may be different than the ground state masses.

Suppose ε is the kinetic energy of the projectile inducing a reaction on a stationary target. Then, this energy is not fully available to be dissipated in the reaction; instead some amount of energy $(\in_{CM})$ must be carried away by the center of mass (CM), where

$$\in_{CM} = \left(\frac{m_x}{m_x + m_T}\right)\varepsilon \qquad 2.2$$

The total energy available for dissipation in the reaction is Q + $\in_0$, where $\in_0 = \varepsilon - \in_{CM}$, or $\in_0 = m_T\varepsilon/(m_x + m_T)$. Then, the necessary but-not-sufficient-condition to start the reaction becomes Q + $\in_0 \geq 0$. From this, we can find that the condition for a reaction to occur is

$$\varepsilon \geq -Q\left(\frac{m_T + m_x}{m_T}\right) \qquad 2.3$$

This minimum kinetic energy that the projectile must have to make the reaction go is called the *threshold-energy* of the reaction. We can see from eqn. 2.3 that for an endoergic reaction, the larger the value of –Q, the larger is the threshold energy.

2.2. Partial wave analysis of reaction of cross-section

Nuclear reaction cross-section is defined as the ratio of the number of particular types of events per time per nucleus to the number of incident particles per time per unit area. It is a measure of amount of interaction. It has the dimension of area and is usually measured in barn (b); where $1b=10^{-28}\ m^2$.

Consider the reaction of an uncharged particle (a neutron) with a target nucleus (T), in which the neutron (n) makes a grazing collision with the target nucleus. Classically, the cross section of T to n would be πb^2, where b is the impact parameter. Angular momentum (L) of the system is normal to the relative linear momentum (p). Applying classical mechanics to this problem, we can write for the impact parameter (b) of the reaction as b = L/p. In the realm of quantum mechanics, linear momentum is quantized and impact parameter is expressed in terms of de Broglie wavelength $(\lambda\!\!\!^{-} = \hbar/p)$ as

$$b = L/p = \ell\lambda\!\!\!^{-} \qquad 2.4$$

where $\ell = 0, 1, 2, \ldots$.

Therefore, since ℓ is quantized so does b. We can associate b with certain rings or zones on the target as shown in Figure 2.1.

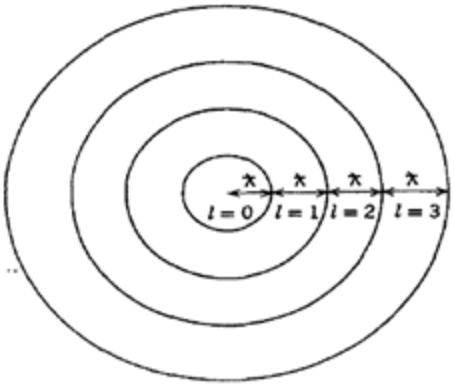

Figure 2.1: Representation of impact parameter on a target nucleus.

The figure suggests that for head-on collisions (ℓ = 0), the range of b is from 0 to $\lambda\!\!\!^{-}$ while for $\ell = 1$, the range of b is from $\lambda\!\!\!^{-}$ to $2\lambda\!\!\!^{-}$, or $\ell\lambda\!\!\!^{-} \le b \le (\ell+1)\lambda\!\!\!^{-}$. Thus a large impact parameter, which is associated with large angular momentum, gives large cross-section. Partial cross section for a specific value of ℓ is $\sigma_\ell = \pi(\ell+1)^2\lambda\!\!\!^{-2} - \pi\ell^2\lambda\!\!\!^{-2}$, or

$$\sigma_\ell = \pi\lambda\!\!\!^{-2}(2\ell+1) \qquad 2.5$$

The total reaction cross-section is $\sigma = \sum_{\ell=0}^{\ell_{max}} \pi\lambda\!\!\!^{-2}(2\ell+1)$. Using series summation,

$$\sigma = \pi\lambda\!\!\!^{-2}(\ell_{max}+1)^2 \qquad 2.6$$

Using $\ell_{max} = R/\lambda\!\!\!^{-}$ into eqn. 2.6, where ℓ_{max} is the maximum value of ℓ, we obtain

$$\sigma = \pi(R+\lambda\!\!\!^{-})^2 \qquad 2.7$$

Since the wavelength $\lambda\!\!\!^{-}$ is related inversely to $\varepsilon^{1/2}$ as $\lambda\!\!\!^{-} = \hbar(2m\varepsilon)^{-1/2}$, we can conclude that at high energies, $\lambda\!\!\!^{-} \ll R$ and hence $\sigma \approx \pi R^2$, which is the geometric cross-section of the nucleus. At low energies, $\lambda\!\!\!^{-} \gg R$ and hence $\sigma \approx \pi\lambda\!\!\!^{-2}$.

Considering neutron wave incident upon the target nucleus, the wave is partially reflected and partially transmitted. Therefore, the expression for the reaction cross-section in quantum mechanics should be modified as

$$\sigma = \pi\lambda\!\!\!^{-2}\sum_{\ell=0}^{\infty}(2\ell+1)T_\ell \qquad 2.8$$

where T_ℓ is the transmission coefficient that varies between 0 and 1.

The transmission coefficient is defined as the ratio of the transmitted wave to the total incident wave. The transmission coefficient expresses the probability that a given angular momentum ℓ transfer will occur. If $\varepsilon \gg V_0$, where V_0 is nuclear potential then $T_\ell = 1$ and $\sigma \approx \pi R^2$. If $\varepsilon \ll V_0$, then $T_\ell \propto \varepsilon^{1/2}$ and the cross-section is $\sigma \propto \pi \lambda^2 \varepsilon^{1/2}$, or

$$\sigma \propto \varepsilon^{-1/2} \propto v^{-1} \qquad 2.9$$

which is the famous 1/v law. Figure 2.2 summarizes the variation of reaction cross-section with kinetic energy of neutron projectiles.

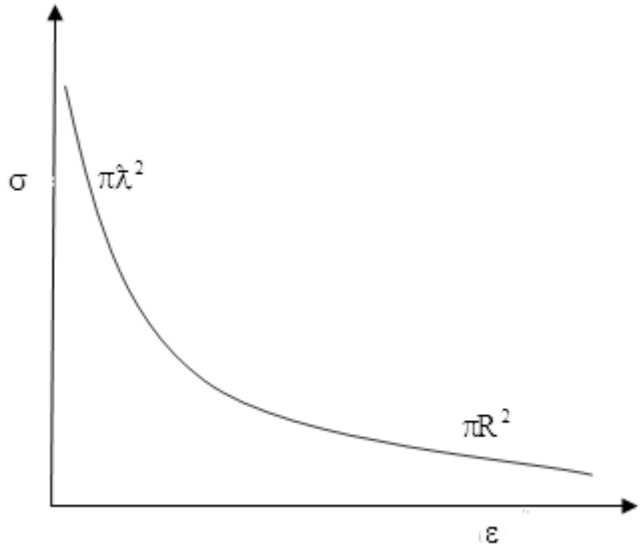

Figure 2.2: Variation of reaction cross-section with projectile energy.

Now let us consider the interaction of a charged particle with a nucleus. As the projectile approaches the target nucleus, it feels the long range Coulomb force and is deflected. As a consequence, the range of collisions corresponds to a smaller range of impact parameters. If the incident projectile has energy ε at an infinite separation from the target nucleus, at the distance of closest approach R, it has a kinetic energy of ε - B, where B is the Coulomb barrier. For a charged projectile, the Coulomb barrier is approximated as the potential between a point charge Z_1e and a homogeneous charged sphere of charge Z_2e and radius R as $B = kZ_1Z_2e^2 / R$.

At the point of closest approach, the linear momentum of the projectile can be written as $p = \sqrt{2\mu(\varepsilon - B)}$, where μ is the reduced mass, $\mu = A_1A_2/(A_1+A_2)$. Classically we have for the maximum orbital angular momentum, $L_{max} = Rp = R\sqrt{2\mu\varepsilon(1-B/\varepsilon)}$, and from quantum mechanics, we have $L_{max} = \ell_{max}\hbar$. Combining these two equations, we obtain

$$\ell_{max} = \frac{R}{\hbar}\sqrt{2\mu\varepsilon\left(1-\frac{B}{\varepsilon}\right)} \qquad 2.10$$

Then using eqn. 2.10 into $\sigma = \pi\lambda\!\!\!^{-2}(\ell_{max}+1)^2 \approx \pi\lambda\!\!\!^{-2}\ell_{max}^2$, we get

$$\sigma = \pi R^2\left(1-\frac{B}{\varepsilon}\right) \qquad 2.11$$

Since σ is always positive, then this equation is valid only for $B \le \varepsilon$.

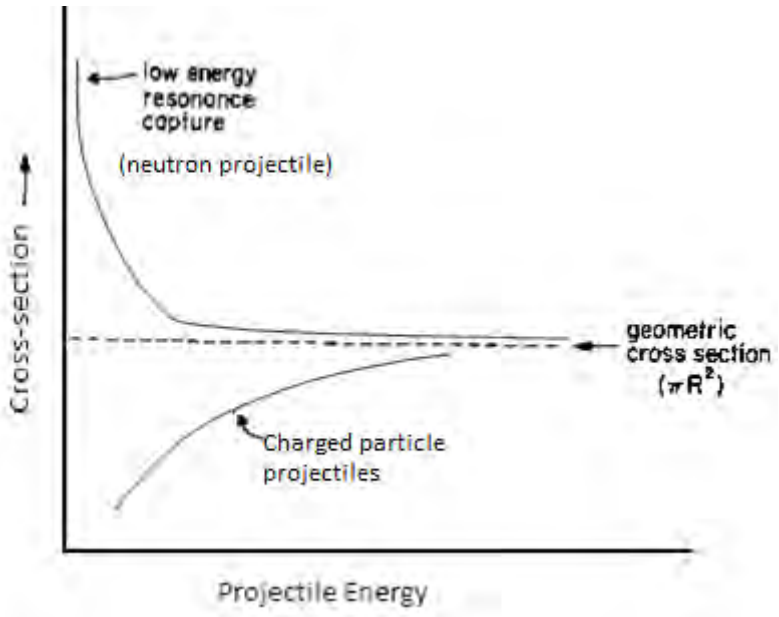

Figure 2.3: Near threshold behavior of neutron and charged particle induced reactions [19].

Equating the reaction barrier B to the Coulomb barrier is applicable to many but not to all charged particle induced reactions since the actual potential felt by an incoming projectile is the sum of nuclear, Coulomb and centrifugal potentials. Figure 2.3 shows general properties of cross-sections for charged and uncharged particles near threshold energies.

2.3. Mechanisms of nuclear reaction

Depending on the mechanism through which a nuclear reaction takes place, the time scale on which it occurs is different; the degree to which the kinetic energy of the incident particle is converted into internal excitation energy of the final products is different and the nature of dependence of the cross-section of nuclear reactions on the energy of the incident particles is also different.

Reaction processes can be subdivided according to time scales or, equivalently, the number of intra-nuclear collisions taking place before emission. A large fraction of nuclear reactions observed has properties consistent with those predicted by two reaction mechanisms which represent the extremes in this general classification. These are the mechanisms of compound nucleus reactions and direct reactions.

In the first group the bombarding particle is captured by the target nucleus to form an intermediate state - the *compound nucleus*. The compound nucleus formation is relatively a long lived process and as a result the subsequent decay of this intermediate state is largely independent of the mode of formation. Thus a given compound nucleus may be formed by several different reactions but the probability of a certain type of final state is only dependent upon the amount of excitation energy.

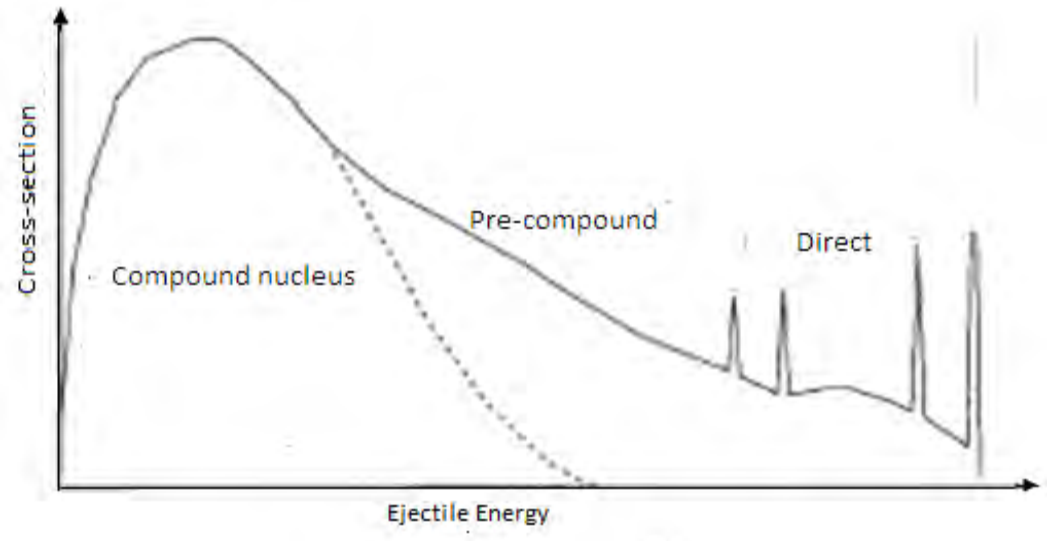

Figure 2.4: Neutron emission spectrum for different nuclear reaction mechanisms [5].

The second type of reaction does not involve the formation of an intermediate state and so in this case the characteristic time of interaction is more of like 10^{-22} s. Figure 2.4 represents neutron emission spectrum showing contributions of different reaction

mechanisms in nuclear reaction. From the figure, the broad peak at low energies shows compound nucleus formation, the sharp peaks at high energies correspond to direct reactions and the region in between the two is the pre-equilibrium region.

2.3.1. Compound nucleus reaction mechanism

Compound nucleus theory is generally given in short as

$$a + X \rightarrow C^* \rightarrow Y + b \qquad 2.12$$

where 'a' is the projectile, 'X' is the target nucleus, C* is excited compound nucleus, 'Y' is the residual nucleus and 'b' is the emitted particle.

A simplified picture of the formation of compound nucleus is that the positive energy projectile particle 'a' is momentarily trapped by a single particle virtual state inside the target nucleus 'X'. Through collision with nucleons inside the target nucleus it shares its energy with them, raising some of them into excited states and itself dropping into one of these states by virtue of the energy it loses [18]. This is the formation of the many particle excited state which is the *compound nucleus* C*. At this stage all memory of the original mode of excitation is lost. At a later time a decay possibility occurs when the energy of excitation is once more concentrated in a single or few particle virtual states. In the evolution of the many-particle excited states several such fleeting decay configurations may occur before one of them is realized and the products separate out into the residual nucleus 'Y' and the emitted particle 'b'. If 'Y' has enough energy, more emissions can occur, otherwise it will de-excite by $\beta-$ or $\gamma-$ emission.

The compound nucleus system involves much longer scales, as the energy of the captured projectile has to be distributed over all particle states in the target. Thus the time scale of compound nuclear reactions is of the order of 10^{-18} – 10^{-16} sec. The reaction duration clearly depends very much on the incident energy, since higher incoming energy transfers more energy into the system and makes it easier to give one nucleon enough energy to escape, therefore giving the compound system formed at higher energy a shorter lifetime. Lifetimes as long as 10^{-14} s have been observed at very low incident energies and lifetimes between 10^{-21} - 10^{-20} s are observed for higher energies. These time scales are very long compared to the time of passage (~10^{-22} s). The very long mean time from the uncertainty relation, $\tau \approx \hbar / \varepsilon$, may indicate that compound nucleus decay takes place at lower energies compared to other reactions.

The compound nucleus theory was proposed by Bohr in 1936 [3]. Bohr divided nuclear reaction in two steps:

i. Mode of formation of the compound nucleus, and
ii. Independent decay of compound nucleus.

According to Bohr, since the lifetime of the compound nucleus is much greater compared to the nuclear time scale, it totally forgets its way of formation. Bohr's idea about the total loss of memory is not completely true. Actually, it is assumed that the mode of decay of compound nucleus is independent of its mode of formation, except for requirement of the various conservation laws. The decay does not depend upon the nature of the incoming particle, but it depends on some quantum mechanical parameters such as the excitation energy, angular momentum, parity of states, etc. therefore, to calculate the cross-section of a complete nuclear reaction, it is necessary to determine two quantities: the formation cross-section and the probability that the compound nucleus decays by emitting particle(s). Then, the cross-section for the complete reaction is expressed as a product of these two quantities. The decay process can be treated statistically on the assumption that the probability of decay by the emission of different types of particles such as protons, neutrons, etc., is the same.

The total cross-section $\sigma(a,b)$ for the complete reaction X(a,b)Y can be expressed as

$$\sigma(a,b) = \sigma_C(a).G_C(b) \qquad 2.13$$

where σ_C is the formation cross-section, $G_C(b)$ is probability that compound nucleus decays with emission of b leaving final nucleus Y, and it is assumed that $G_C(b)$ is independent of the mode of formation of the compound nucleus.

Consider the case that the compound nucleus C* decays by emitting a different particle d leaving a residual nucleus Z, the total cross-section for the complete reaction X(a,d)Z becomes $\sigma(a,b) = \sigma_C(a).G_C(d)$. Thus, for the same energy, angular momentum and parity, we assume the same formation cross-section $\sigma_C(a)$.

Let the mean life of C* be τ, the full width at half maximum satisfies the relation $\Gamma.\tau = \hbar$. If Γ_a, Γ_b, Γ_d, ... are partial widths of the modes of decay a, b, d, ..., respectively, where $\Gamma = \Gamma_a + \Gamma_b + \Gamma_d$ ..., then we can express the decay rate through the channel b as

$$G_C(b) = \frac{\Gamma_b}{\Gamma} \qquad 2.14$$

Since the formation and decay of a compound nucleus are two independent processes, according to Bohr's assumption, it is possible to find a relationship between Γ_b and $\sigma_C(b)$. From reciprocity theorem we can say that

$$k_a^2\sigma(a,b) = k_b^2\sigma(b,a) \qquad 2.15$$

where k_a and k_b are wave numbers in 'a' and 'b' channels, respectively.

Then, the total cross-section of the overall compound nucleus reaction can be given as

$$\sigma(a,b) = \sigma_C(a).\frac{\Gamma_b}{\Gamma} \qquad 2.16$$

From the above relations, we can derive a constant function U as

$$U = \frac{k_a^2\sigma_c(a)}{\Gamma_a} = \frac{k_b^2\sigma_c(b)}{\Gamma_b} \qquad 2.17$$

where U is a function only of state, that is, angular momentum, energy and parity of compound nucleus, but independent of the channel. Using the above equations, decay probability given by eqn. 2.14 becomes

$$G_C(b) = \frac{k_b^2\sigma_C(b)}{\sum k_a^2\sigma_c(a)} \qquad 2.18$$

Using eqn. 2.18 into eqn. 2.16, the total cross-section for the compound reaction is

$$\sigma(a,b) = \sigma_C(a).\frac{k_b^2\sigma_C(b)}{\sum_{a'} k_{a'}^2\sigma_C(a')} \qquad 2.19$$

The validity of Bohr's hypothesis was demonstrated by several experimenters. One of them is Ghoshal classical experiment [3]. Ghoshal produced the same compound nucleus $^{64}Zn^*$ by bombarding ^{63}Cu with a proton beam and ^{60}Ni with alpha beam. His reactions were

$$^{63}Cu(p,n)\,^{63}Zn \quad ^{63}Cu(p,pn)\,^{62}Cu$$
$$^{60}Ni(\alpha,n)\,^{63}Zn \quad ^{60}Ni(\alpha,pn)\,^{62}Cu$$

We can have relationships among these different reactions as follows. Using eqn. 2.19 for (p,n), (p,np), (α,n) and (α,np) reactions, we have

$$(i)\,\sigma(p,n)=\sigma_C(p).\frac{k_n^2\sigma_C(n)}{\sum_{a'}k_{a'}^2\sigma_C(a')} \qquad (iii)\,\sigma(\alpha,n)=\sigma_C(\alpha).\frac{k_n^2\sigma_C(n)}{\sum_{a'}k_{a'}^2\sigma_C(a')}$$

$$(ii)\,\sigma(p,np)=\sigma_C(p).\frac{k_{np}^2\sigma_C(np)}{\sum_{a'}k_{a'}^2\sigma_C(a')} \quad (iv)\,\sigma(\alpha,np)=\sigma_C(\alpha).\frac{k_{np}^2\sigma_C(np)}{\sum_{a'}k_{a'}^2\sigma_C(a')}$$

Taking the ratio of (i) to (iii) and the ratio of (ii) to (iv), we get

$$\sigma(p,n)/\sigma(\alpha,n)=\sigma_C(p)/\sigma_C(\alpha)$$
$$\sigma(p,np)/\sigma(\alpha,np)=\sigma_C(p)/\sigma_C(\alpha)$$

The right hand side expressions of these two equations are the same. Therefore,

$$\sigma(p,n):\sigma(p,np)=\sigma(\alpha,n):\sigma(\alpha,np) \qquad 2.20$$

To produce the same excitation in $^{64}Zn^*$, an additional 7 MeV was added to the kinetic energy of protons $\left(\varepsilon_\alpha=\varepsilon_p+7MeV\right)$. Since excitations produced through the two processes are the same, the decay probability $G_C(b)$ is also the same, for it depends only on the excitation produced in the compound nucleus.

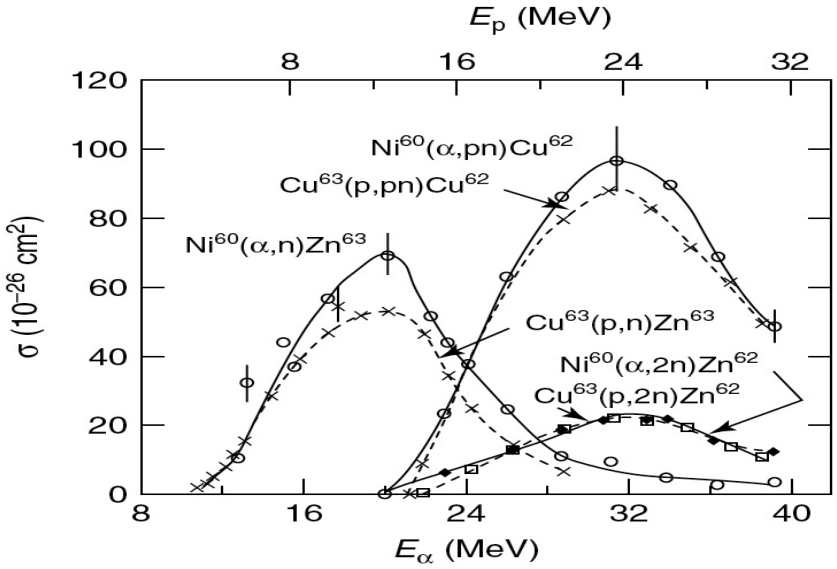

Figure 2.5: Ghoshal experimental verification of Bohr's theory [3].

Formation and decay of a compound nucleus reaction mechanism can be visualized in the liquid drop model, in which the two colliding droplets combine to form a single drop (the compound nucleus). Since the compound nucleus is excited, it has high temperature and its decay is thought of as the cooling of this drop, which takes place by evaporation of one or more of the constituent particles.

In the energy/momentum transfer process, during compound nucleus formation, there is concentration of energy on any one particular nucleon. This nucleon is emitted if it gains an amount of energy more than the separation energy per nucleon (S), which is nearly equal to the binding energy (E_B). Therefore, for compound nucleus decay to take place, total excitation energy of the compound nucleus, which is given by $E = \varepsilon + E_B = \varepsilon + S$, must be much less than the total separation energy (AS) of nucleons. That is, $AS \gg \varepsilon + S$. If the kinetic energy of the incident particle is not too high (ε < 50 MeV), its mean free path (Λ) in a nuclear matter is very much smaller than the nuclear radius (R). Therefore, the necessary but not sufficient conditions for the validity of Bohr's assumption are

$$\Lambda \ll R \quad \text{and} \quad \varepsilon \gg (A-1)S \qquad 2.21$$

That means, compound nucleus decay takes place if the kinetic energy of the projectile is very much smaller than the total separation energy on the nucleons and the mean free path should be very much smaller than the nuclear radius (R). If the mean free path is very much small, the energy of the projectile is quickly shared among the A constituents of the compound system so that each of them possesses on the average the amount E/A. The mean free path in a nuclear interaction can be given as

$$\Lambda(\text{in cm}) \gg \begin{cases} 4.0\times10^{-14}, \text{ for } \varepsilon \le 20\,\text{MeV} \\ 1.8\times10^{-15}\times E(\text{MeV}), \text{ for higher } \varepsilon \end{cases} \qquad 2.22$$

We can see from eqn. 2.22 that Λ increases with increasing excitation energy at higher projectile energies greater or equal to 20 MeV only.

Both conditions are fulfilled for nuclei with A > 10 so long as $\varepsilon < 50\,\text{MeV}$, since S is of the order of 8 MeV. We can also infer that for light targets, compound nucleus decay takes place only at low energies (< 20 MeV). However, for heavy targets, equilibrium decay takes place at low and medium projectile energies.

Level density models for processes involving evaporation

The need to determine the quantity level density is because it is useful to estimate the cross-section of a nuclear reaction, according to Hauser-Feshbach theory [2]. Nuclear level density is defined as the number of levels per unit energy at certain excitation energy. If the excitation energy lies in the range E to E+dE, then the average level density is defined as $\rho(E) = dN/dE$. In other words, it is the number of different ways in which individual nucleons can be placed in the various single particle orbitals.

We do not have data for every nucleus in wide range of excitation energy and angular momentum so we have to largely depend on models to predict the nuclear level density. Two frequently used models for such evaporation processes are the *Fermi-gas* model and the *constant temperature* model. These models depend on excitation energy and they consider the fact that fermions have the tendency to form pairs and hence extra amount of energy is needed to separate them. Taking this into account while calculating level densities, a shift δ is done on the excitation energy (i.e., $U = E - \delta$).

The *Fermi-gas model* is applicable at high excitation energies (above the matching point U_x). In this model, level density $\rho_F(U)$ is described in terms of the excitation energy U as

$$\rho_F(U) = \frac{\sqrt{\pi}}{12}\frac{\exp\left(2\sqrt{aU}\right)}{(aU^5)^{1/4}} \qquad 2.23$$

where 'C' is the proportionality constant and 'a' is called level-density-parameter and is defined as $a = A_{CN}/K$, where A_{CN} is the mass of the compound nucleus and K is an adjustable constant. The parameters 'a' and 'δ' differ from nucleus to nucleus and can be adjusted in order to agree with the values of the level densities at lower energies and at the nucleon separation energy.

The *constant temperature model* is applicable at low excitation energies (below the matching point U_x) and is given by

$$\rho_T(U) = \frac{1}{T}\exp\left[(U - E_0)/T\right] \qquad 2.24$$

where T is the nuclear temperature and E_0 is an adjustable energy shift.

Charged particle induced reactions

If the emitted particles are neutrons in a reaction involving evaporation, the emitted neutron energy spectrum has the form

$$N(\in)d\in = \frac{\in}{T^2}\exp\left[-\in/T\right]d\in \qquad 2.25$$

where $\in$ is energy of the emitted particle. We can see that the particles are emitted with a Maxwellian energy distribution as shown in Figure 2.6.

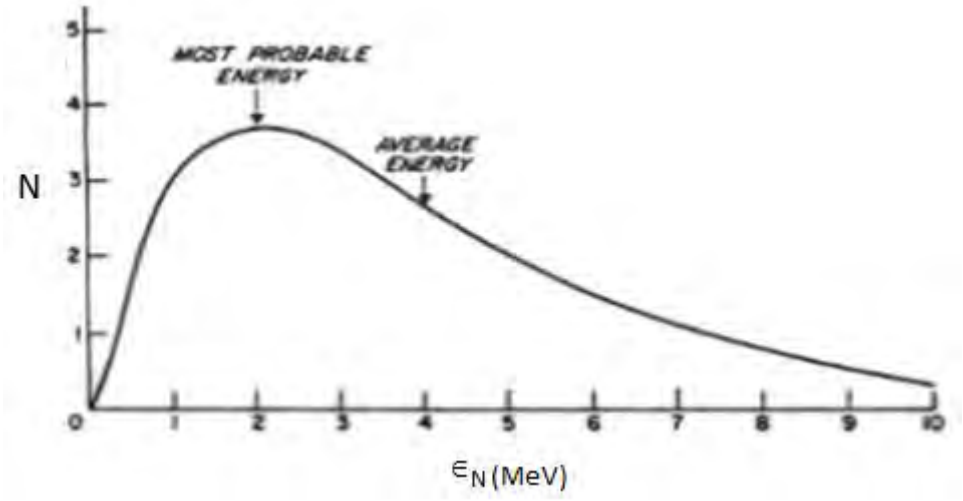

Figure 2.6: Spectrum of evaporated neutrons.

What we are saying is that the compound nucleus "evaporates" particles like molecules leaving the surface of a hot liquid. Note that for charged particle evaporation, eqn. 2.25 will be modified by replacing the term $\in$ by $\in - \in_S$, where $\in_S$ is threshold energy of charged particle emission which is approximately the Coulomb barrier.

The energy variation of the cross-section (the excitation-function) for processes involving evaporation is fairly distinctive as shown in Figure 2.7, where the excitation function for the ^{209}Bi(α,xn) reaction is shown. The cross-section rises with increasing energy because the formation cross-section for the compound nucleus is increasing according to eqn. 2.12. Eventually the excitation energy of the compound nucleus becomes large enough that emission of two neutrons is energetically possible. This "2n out" process will dominate over the "1n out" process and the cross-section for the "1n out" process will decrease. Eventually the "3n out" process will dominate over the "2n out" process.

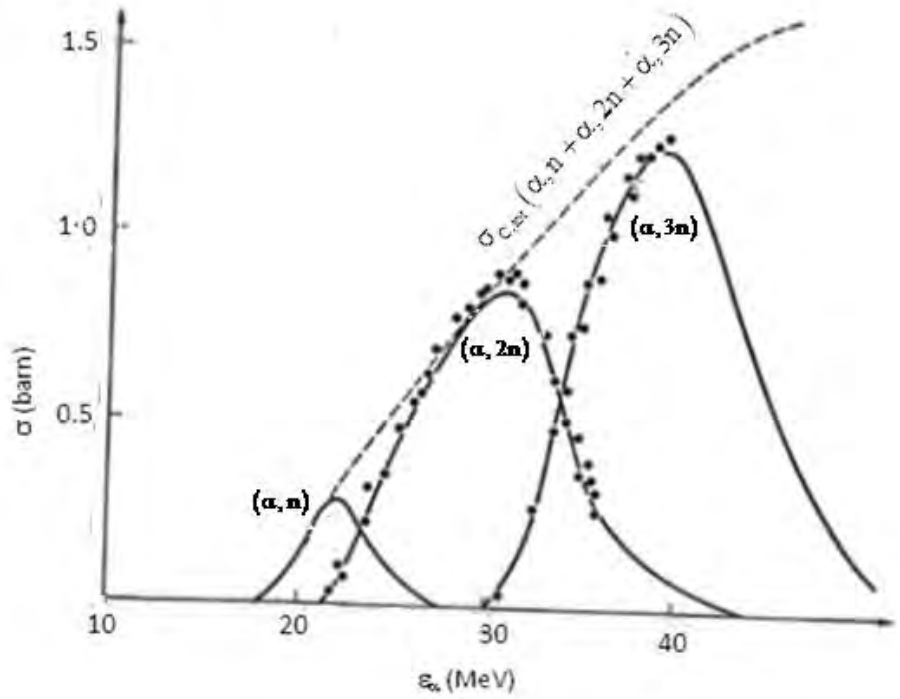

Figure 2.7: Excitation function for the ^{209}Bi(α,xn) reactions.

EQ excitation functions for p+V and p+Bi reactions

Let us assume that because the compound nucleus has "forgotten" its mode of formation, there should be no preferential direction for the emission of the decay products. As discussed above, for the reaction a + A → C* → b + B, if P_C is the probability that C* will decay to form b + B. Clearly $\sum P_C(b) = 1$. Therefore, the variation in cross-section with projectile energy is due to the variation in the formation cross-section only.

The Coulomb barriers on the proton induced reactions on bismuth and vanadium targets are determined by inserting proper values of the corresponding nuclides into eqn. 2.10. The semi-classical reaction cross-sections of the two reactions are then determined using eqn. 2.12. Thus,

$$\sigma = \begin{cases} 2.18\left(1 - 14.4/\varepsilon\right), & \text{for } ^{209}\text{Bi} \\ 1.01\left(1 - 5.9/\varepsilon\right), & \text{for } ^{51}\text{V} \end{cases} \qquad 2.26$$

where ε's are in MeV and σ's are in barn (b). Threshold energies are 5.9 MeV and 14.4MeV for vanadium and bismuth targets, respectively.

We can compare heights of the two excitation functions by calculating the inequality $\sigma_V - \sigma_{Bi} \geq 0$, where σ_V and σ_{Bi} are cross-sections of the corresponding reactions given in eqn. 2.26. Thus, solving $\left(25.3\,\text{MeV}/\varepsilon\right) - 1.18\,\text{MeV} \geq 0$ for ε, we obtain

$$\varepsilon \leq 21\,\text{MeV} \qquad 2.27$$

This means that for processes involving evaporation, the reaction cross-section of $p+^{51}V$ is higher than $p+^{209}Bi$ reaction at any proton energies below 21 MeV.

2.3.2. Direct reaction mechanism

In direct reactions (or peripheral reactions), the incident particle interacts primarily with few nucleons at the surface of the target nucleus and it proceeds directly from the entrance channel to the exit channel without the formation of any intermediate state. Therefore, there is a strong correlation between the initial and final channels of the reaction. Direct processes are characterized by short reaction times, which is roughly equal to the time it takes the incident particle to traverse the target nucleus (~ 10^{-22} seconds).

A very small life time of the projectile-target system, termed as the time of passage, $R\left(2m/\varepsilon\right)^{1/2}$, implies that direct reactions undergo at higher incident energies, where R is nuclear radius and m is projectile mass. For incident energies above about 10 MeV, the low-lying, discrete states of the residual nucleus are almost completely excited by direct reaction processes. The associated angular distributions are strongly peaked in the forward direction (resulting in particle forward peaking) and exhibit markedly oscillatory behavior. High incident energy in direct processes also implies that direct reactions involve a very small number of the available degrees of freedom. This is because, as the energy of an incident particle increases, its de Broglie wavelength, $\lambda\!\!\!^{-} \approx \hbar\left(2m\varepsilon\right)^{-1/2}$, decreases until it becomes more likely to interact with a nucleon sized particle than with a nucleus sized object.

In most direct reactions, pick-up or stripping reactions are observed. That is one or more nucleons may transfer from the target nucleus to the incident particle or vice versa, respectively. These transfer type reactions leave the two partners in their ground states or in one of their many excited states.

We may also have direct reactions in which the final products are the same chemical copies of the reactants. Such reactions may be either elastic or in-elastic scattering. In an elastic scattering, the interacting system remains in its initial quantum mechanical parameters except negligible energy loss for conservation of linear momentum. In an in-elastic direct reaction, only the target nucleus is excited. After a while, this excited residual nucleus will immediately de-excite by γ-emission.

Pre–equilibrium reaction mechanism

Experimental results showed that a nuclear reaction mechanism has also intermediated characters between direct and compound nucleus reactions. The cross-section as predicted by the pure compound process is too small with respect to the measured spectrum. Furthermore, the measured angular distributions in this intermediate region are anisotropic, indicating the existence of a memory-preserving, direct-like reaction process. Such reaction type that embodies both direct- and compound-like features is referred to as *pre-equilibrium* or *pre-compound* or, usually in a quantum mechanical context, *multi-step processes*. Pre-equilibrium decay is expected to be responsible for the experimentally observed high-energy tails.

2.3.3. The exciton model

The term exciton refers to the excited degrees of freedom, i.e., to the number of excited particles and holes. If the excitation energy is shared between p particles and h holes then the exciton number n is written as n = p + h.

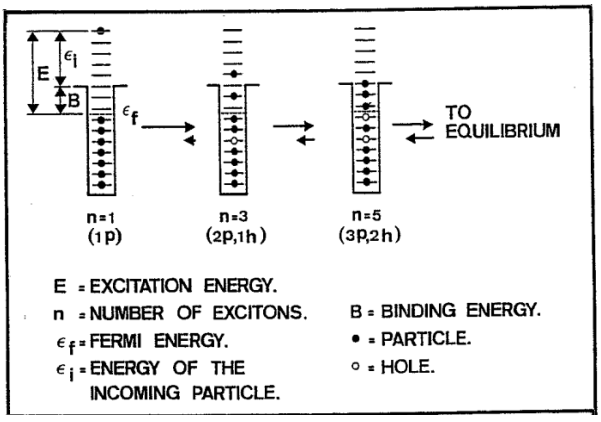

Figure 2.8: Representation of the equilibration process as formulated in the exciton model.

In Figure 2.8, the nuclear potential is shown with equally spaced single particle levels, i.e., levels whose occupancy is either 0 or 1. Initially the target nucleus is in the ground state. All levels below the Fermi energy ε_f are filled and all levels above are vacant. A nucleon projectile with a given energy enters the target nucleus and forms a 1 particle - 0 hole (1p-0h) state, i.e., a state with exciton number n = 1. At this stage, the projectile is still in the entrance channel but has entered the nuclear force field. It may interact or may leave the nuclear force field without interacting with any individual target nucleon. Since all levels below the Fermi energy are filled, the first interaction between the projectile and a target nucleon will raise the latter above the Fermi energy and leave a hole below. Thus, a 2p-1h state is formed. In other words, the absorption of the projectile nucleon by the target leads to the formation of an n = 3 exciton state.

After formation of n = 3 state, subsequent interactions result in changes in the number of excitons, characterized by $\Delta n = +2$ (a new particle-hole pair) or $\Delta n = -2$ (annihilation of a particle-hole pair) or $\Delta n = 0$ (creation of a different configuration with the same exciton number). In the first stage of the process, corresponding to low exciton numbers, the $\Delta n = +2$ transitions are predominant. However, at any stage there is a non-zero probability that a particle is emitted. Hence, in principle the exciton model enables to compute the emission cross-sections in a unified way, without introducing arbitrary adjustments between equilibrium and pre-equilibrium contributions.

CHAPTER 3

THE COMPUTER CODES

Various models have been proposed to understand nuclear reaction mechanisms using a variety of computer codes. These computer codes are used to predict and analyze different products of nuclear reactions; to verify the mechanisms of nuclear reactions; to help in the identification of compound nucleus formation and decay; to determine angular momenta and to search for non-statistical aspects of nuclear structures at higher excitation energies and higher angular momenta.

On the basis of statistical models, we can do theoretical calculations using different computer codes such as COMPLET, Pace-4, etc. The nuclear level density of a nuclide in the evaporation chain may be calculated from the Fermi density distribution given by eqn. 2.23 in chapter 2. The Q Value for the formation of the compound nucleus and the neutron, proton, deuteron binding energies for all nuclides of interest in the evaporation chain, has been calculated using Myers-Swiatecki/Lysekil mass formula [9]. The inverse reaction cross-section is calculated from optical model and the mean free path multiplier for intra-transition rates are calculated from optical potential parameters.

3.1. The COMPLET Code

In this thesis, theoretical calculations were done using the code COMPLET. This code was designed for versatility and ease to use in the bombarding energy range of a few MeV to several hundred MeV. Taking two mechanisms (equilibrium and pre-equilibrium) into account, it predicts the yield of residual nuclei in nuclear reactions with excitation energies up to 225 MeV. The pre-equilibrium emission is accompanied in the frames of the model of independently interacting excitons. An approximation concerning Pre-equilibrium angular momentum removal is included. The equilibrium part formerly based on Weisskopf–Ewing evaporation formula is also modified to include full angular momentum decoupling regarding emission of light particles with $A \leq 4$. In pre-equilibrium processes, the particles in the initial configuration $\left(n_0 = Ex1 + Ex2 + Ex3\right)$ can be neutrons, protons or alpha particles, represented by the exciton numbers Ex1, Ex2 and Ex3, respectively. It is customary to use the initial exciton number n_0 separated into proton and neutron above and holes below the Fermi level as a fit

parameter to match theoretical predictions with experimental excitation function. The requirement of detailed input parameters was sacrificed to achieve this goal. The code COMPLET provides yields and spectra for all reactions populated by all combinations of n, p, d, α and can provide all input parameters internally. This code includes damping of fission widths above a critical temperature R_0. The code used is a further simplification of the formula by Paul and Thoennessen in Ann.Rev.Nucl and particle science 44(1944).

The version needs only about 2 megabyte of memory. Therefore, it has the option to calculate particle-residual nucleus correlations as well as inclusive p- and n-spectra. The code complet includes pre-equilibrium neutrons, protons and alpha emission up to two particles, as well as evaporation of neutrons, protons, alpha particles, deuterons, tritons and hellions.

The code COMPLET is based on the same philosophy as the former code *index*. It applies the statistical model of compound nucleus decay developed by Weisskopf–Ewing, and the hybrid/geometric dependent model [8] of Blann for pre-equilibrium decay processes after further simplifications and improvements are done by J. Ernst. This code helps to predict the excitation functions of pure equilibrium decay as well as pre-equilibrium decay. Originally, this code has been developed out of the code overlaid Alice by M. Blann. While some standard routines remained practically unchanged (like Fisrot, Lmass, Punch, PLt, Parap, Over1, Over2 and TLj), others have been substantially modified (like Main, Shaft, Nucmfp, etc.) or are completely changed (like, Index, Parden, Trapro, Angular, etc.). The underlying PE-MODEL is described in Z. Phys. A328 (1989). It is contained in subroutine index.

3.2. Description of input parameters

Values used for input parameters are

Reals for CN and PE: AP =1.0, AT = 209.0 for Bi, 51.0 for V, ZP =1.0, ZT = 83.0 for Bi, 28.0 for V, QVAL = 0.0, PLD = 8.0 -14.0, CLD = 1.0, RO = 0.0, GI = 0.0, G0 = 0.0, EKIN = 7.0 - 70.0 MeV, RCSS = 0.0

Reals for PE: TD= 3.0, EX1= 1.0, EX2= 1.0, EX3 =0.0, POT=0.0, AV=0.0, ALF=0.20, CMFP =0.5, 1, 2, or 3, GDO = 0.0

Integers for CN and PE: NA = 10, NZ = 9, MC = 0, MP = 0, IPA = 0, M3 = 3, INVER = 1, IKE = 1, IPCH = 0, KPLT = 0

4 CN and 1 PE integers: JCAL=1, JFRAC, JUPPER, JANG = 99 , IJ =1

The input parameters for the full operation of the program are summarized below. The notion “card” from the old FORTRAN input is still kept but now corresponds to lines. Free formats, the input values should be separated by ”,” or “CR”.

Card 1

General input data: definition of scattering system and calculation method. Symbol description

AP- Projectile Mass number

AT-Target Mass number

ZP-projectile charge

ZT-Target Charge

QVAL – Reaction Q value = AP + AT - ACN.

=0: calculated from M and S Mass formula

= 1: calculated from mass excesses of 1990 nuclear wallet cards

CLD–ratios of single particle level densities af/an = 0: af/an=1

If parameter ISOT is nonzero, CLD is isotopic abundance input default value =1.0

If = 0, use rotating finite range fission barriers due to A. J. Sierk

BARFAC- multiplies the rotating drop fission barrier by this value.

BARFAC = 0: BARFAC = 1

ROFFAC – multiplies the rotational energy by this value = 0;

ROTFAC = 1

RO- Critical temperature above onset of retarded fission

GI – nuclear friction parameter from equilibrium deformation to saddle

G0- nuclear friction parameter from saddle to scission point

NA – the number of nuclides of each Z to be included in the calculation. Up to 21 neutrons may be emitted (maximum NA=22)

NZ - the number of Z–values to be calculated in the emission process. Up to 8 protons may be emitted (maximum NZ=9)

For correct PE calculation binding energies are calculated for all nuclei with IZ,IA≤5

MC – shell correction option for masses subroutine

MC – O, masses incl. shell correction

MC = 1, masses without shell correction term

MC = 2, BE values will be supplied as input.

MC > 2, BE values are calculated from 1990 nuclear wallet cards.

MP – pairing correction to masses

MP = 0: no pairing term in masses

MP = 1: pairing term in masses, 1dgs calculated from ms1 formula and applied back shifted

MP = 2: masses are from nuclear wallet cards;

MP = 3: pairing correction in masses, NOTE: changes are not corrections in only level densities

IPA – pairing corrections in level densities

IP = -1, no corrections

IP = 0, standard correction i.e. multiplier = 12

IPA > 0 multiplier is IPA

M3 – number and type of particles to be emitted from each nuclide

If =1: N only;=2:N and P;=3 or = 0:N,P and Alpha; =4;N,P, Alpha and Deuteron

If = 5:N, P, Alpha Deuteron and Triton = 6: N,P, Alpha Deuteron Triton and hellion (3HE)

If = 7: as before incl. Gammas. Calculations until gamma emission are finished important for isomeric ration calculations.

INVER- inverse cross-section parameters

If = 0: user supplied:

If = 1: results by O.M subroutines as ALICE/85/300,

If = 2: O.M for N,P as in old ALICE

If = 3: sharp cut off values for inverse cross-section

Option Inver = 2 greatly reduces total cup time

IKE if =1 no particle spectra will be printed

If = 2 equilibrium spectra for each nuclide will be printed:

If = 3 pre-Compound spectra will be printed:

If = 5 PE and summed equilibrium spectra will be (Separately) printed:

If IKE = -2 to -5: reduce output with spectra as IKE = ABS (IKE) (yields are printed after negative energy input):

If$IKE \leq 0$ or $IKE \leq 6$ most reduced output:

Emitting nuclides and all partial waves of pre–Compound plus equilibrium spectra to print gamma spectra, increase the IKE value selected by 5.

If IPCH = 1 or = 2, fission barriers are to be read in after this first record IPCH= -1: inverse cross-sections will be readout for possible future use in separate output file.

= 0: or NE from 1. no print out

KPLT-number of decades to be plotted as excitation functions on line printer. If KPLT= 0: no plotting

Card 2

Title Card-80 Columns

If MC = 2 on CARD 1, read user supplied n, p, alpha, deuteron, triton and hellion binding energies here, Format for IA= 1 to NA, IZ = 1 to ONZ.

If INVER = 0 on CARD 1, read then n, p, alpha, deuteron, triton, hellion and gamma inverse cross-section here

In ascending channel energy first value =0.1MeV, incremented by 1MeV,48 values per-particle type in sequence N,P,A,D,T 3HE, and gamma depending on value of M3

Card3

Energy compound nucleus and pre-equilibrium option

Symbol Description

IKEN: projectile kinetic energy in the Laboratory System.

If = 0: A new problem will begin at Card 1

If<0: previously Calculated excitation functions will be printed (if KPLT= 0, EKIN values were run in ascending order they are plotted)

If EKIN=0 on two successive cards, a normal exit will occur for negative target mass on card 1.

RCSS=0: reaction cross-section is calculated from subroutine (for pi-induced reactions: if RCSS (input)=0, RCSS= 100mb)>: number of T(1) values to read from the next Card JCAL

=1, Weisskopf-Ewing evaporation calculation

=2, S- wave approximation, Liquid drop moment of inertia

= 3, S-wave approximation rigid body moment of inertia (only if entrance Channel cross–sections calculated by parabolic approximation, i.e. ZP >1 and RCSS=0)

= 0, evaporation–fission competition partial wave by partial wave.

JFRAC-direct–semi-direct capture gamma ray estimate :<0: no emission >0: approach of kalka

JANG – JANG +1 = maximum number of contributing incoming partial waves.

Usually use the maximum: JANG = 99. Otherwise JANG can be used for cutoff on L-values provided by subroutines OVER 1 and 2.

All other Parameters on this Card are for the pre-compound calculation options. Put TD-values to Zero if no pre Compound calculation is wanted.

TD- Initial exciton number = P+h

EX1 – Initial excited neutron number.

EX2 – Initial excited proton number

EX3 – Initial alpha particle exciton number

POT- Fermi energy in MeV

If = 0; POT is calculate from nucl. matter value =37.8 MeV

AV-if AV = 0 =1 optical model mean free paths are used in routine MFP. NOT to be used above 55 MeV.

If AV= 1: Nucleon-Nucleon mean free paths are used in NUCMFP.

ALF- probability that newly created exciton particle from first stage exciton sets and alpha particle in the second stage.

(1-ALF): complementary probability

If ALF>1 calculation for two initial exciton numbers

A) ATD = TD-3 (min-1.5) AEX1= AEX2 = 0.AEX3 = 2; ATD = TD-6 for TD>9 with weight ULF = INT (ALF) 100

B) Weight = (1-ULF), with initial exciton numbers.

CMFP – Mean free paths are multiplied by CMFP. If CMFP O: multiplier is 1.

GDO–critical angular momentum. GDO>0: partial Waves with L>GDO are not taken into account in line of isotone cross- sections while cross –sections for partial Waves with L>GDO are accounted for in the line below

N.B for GDO $\leq$ +0.5 No cut off

In these interactions the original exciton type is assumed to be conserved. The newly created exciton may be $\alpha-$particle, $\alpha-$hole state formed with probability (1-ALF). The Value of ALF = 0.2 is found to be the best Choice.

CHAPTER 4

EXPERIMENTAL MEASUREMENT TECHNIQUES OF EXCITATION FUNCTIONS

One method of measurement of cross-sections of proton induced nuclear reactions is just by detecting the emitted particles or radiations (events). To measure excitation functions of proton induced reactions, the single or stacked foil activation technique can be used [10]. In these techniques, target foils are irradiated with proton beam projected by accelerators at various energies. After irradiation, the X-ray or gamma activities induced in each target foils are analyzed using γ-ray and X-ray detectors, respectively. Finally, excitation functions of specific reactions are calculated from the intensities of the characteristic X- rays or γ-rays of particular residual isotope.

4.1. Activation cross-section

The expression for the cross-section of a nuclear reaction may be written from the consideration of decay rate equation governing the nuclear transformation and decay of the activated product. If we consider the situation where a beam of projectile nuclei of constant flux ϕ is incident upon a thin foil of target nuclei, then the rate of production R_p is related to the activation cross-section σ by

$$R_p = \sigma\phi N_0 \qquad 4.1$$

where N_0 is the number of target nuclei of isotope under investigation present in the sample (vanadium or bismuth in our case). It is given by $N_0 = mN_A f / A_0$, where m is mass of the sample, N_A is Avogadro's number, A_0 is the atomic weight and f is the abundance of the isotope in the target.

If the time of irradiation of the target, by the constant flux incident beam to produce a radioactive reaction product R, is t_1, then the differential equation governing the growth of the activity during production is given by

$$\frac{dR}{dt} = \sigma\phi N_0 - R\lambda \qquad 4.2$$

where λ is the decay constant, and λR is the activity of R-type nuclei.

Solving eqn. 4.2 for $W = \lambda R$ by applying integration in the time limits between 0 and t_1, where W is the activity of R-type nuclei at the end of the irradiation, we obtain

$$W = \sigma\phi N_0 \left\lfloor 1 - \exp\left(-\lambda t_1\right) \right\rfloor \qquad 4.3$$

The term, $1 - \exp\left(-\lambda t_1\right)$, is called the *saturation factor* of the reaction.

The growth of decay, at any time 't' after the time 't_1', is $dR/dt = W\exp(-\lambda t)$. Substituting eqn. 4.3 into this and integrating dR with respect to the time limits of t_2 to $t_2 + t_3$, we get

$$D = \int_{t_2}^{t_2+t_3} \sigma\phi N_0 \left[1 - \exp\left(-\lambda t_1\right)\right] \exp\left(-\lambda t\right) dt = \frac{\sigma\phi N_0 \left\lfloor 1 - \exp\left(-\lambda t_1\right) \right\rfloor \left\lfloor 1 - \exp\left(-\lambda t_3\right) \right\rfloor}{\lambda \exp\left(-\lambda t_2\right)} \qquad 4.4$$

where t_2 is the time elapsed between stopping the beam and the start of count, D is the actual number of disintegrations of the sample during a time period of t_3 starting after a time t_2 from the stop of irradiation.

If A is the number of counts observed by the detector during the time interval 't_3', then the actual number of disintegrations can also be given by

$$D = \frac{A}{G\varepsilon.\theta k} \qquad 4.5$$

where 'Gε' is geometry dependent efficiency of the detector, θ is the absolute intensity of the particular gamma ray and k is the self-absorption correction factor of the gamma ray in disk shaped target. It is given by

$$k = \frac{1 - \exp\left(-\mu d\right)}{\mu d} \qquad 4.6$$

where μ is gamma ray absorption coefficient, d is the thickness of the target under investigation. The activation cross-section of a nuclear reaction [10] is obtained by combining eqn. 4.4 and eqn. 4.5, as

$$\sigma = \frac{A\lambda \exp\left(-\lambda t_2\right)}{\phi N_0 \left[1 - \exp\left(-\lambda t_1\right)\right]\left[1 - \exp\left(-\lambda t_3\right)\right] G\varepsilon.\theta k} \qquad 4.7$$

This expression has been widely used to calculate the activation cross-section for the proton induced reactions on different isotopes [10].

4.2. Experimental results

The experimental data were taken from EXFORA IAEA data reference [11]. Authors and reaction types of which data are collected are listed below.

Reaction types	**Authors**
$^{51}V(p,n)^{51}Cr$, $^{51}V(p,3n)^{49}Cr$	R.Michel, G.Brinkmann, H.Weigel, W.Herr [14]
$^{51}V(p,4n)^{48}Cr$	S.Hontzeas, L.Yaffe [17]
$^{209}Bi(p,3n)^{207}Po$, $^{209}Bi(p,4n)^{206}Po$	C.Birattari, E.Gadioli, A.M.GrassiStrini, G.Strini,G.Tagliaferri, L.Zetta [15]
$^{209}Bi(p,n)^{209}Po$, $^{209}Bi(p,2n)^{208}Po$	K.Miyano, H.Nakahara [16]

Theoretical calculations were done using proton energy ranges used in experimental measurements so that comparison between theoretical and experimental excitation functions is simplified. No theoretical calculation is done for $^{209}Bi(p,2n)^{208}Po$ reaction, but the experimental data is used in Figure 5.21 for a general overview.

CHAPTER 5

CALCULATIONS OF EXCITATION FUNCTIONS FOR SOME ^{51}V(P,XN) AND ^{209}Bi(P,XN) REACTIONS

The reaction cross-section calculations are done for compound nucleus decay and pre-compound nuclear reactions using COMPLET code. Theoretical calculations are carried out for three ^{51}V(p,xn) reactions and for four ^{209}Bi(p,xn) reactions. We started comparison on input parameters, then theoretical and measured excitation functions are compared and finally, conclusions are drawn.

5.1. Comparing input parameters

The impact of some input parameters on theoretical cross-section values varies from reaction type to reaction type. In this case, comparisons were done for three input parameters, namely, initial exciton number, level density parameter and mean free path multiplier. It is observed that all the three parameters affect the excitation function of the pre-equilibrium decay, but the equilibrium decay excitation function is affected only by the level density only.

A general agreement is observed between the experimental results and theoretical pre-compound predictions with an initial exciton configuration given by n_0 = 3(1p+1n+1h). The effect of the level density parameter (PLD) on excitation functions was studied by varying the adjustable constant K. In our case, level density parameters between $A_{CN}/8$ and $A_{CN}/14$ are used for different theoretical cross-section calculations. The third tested input parameter was the mean free path multiplier (CMFP). The CMFP values 0.5, 1, 2 and 3 are used for different cross-section calculations.

5.1.1. Effect of PLD on excitation functions

Effects of level density parameter (PLD) were compared for some equilibrium and pre-equilibrium reaction mechanisms. For theoretical pre-equilibrium cross-section calculations, we have used CMFP = 1.00 and n_0=3(1p+1n+1h).

A. $^{51}V(p,n)^{51}Cr$ reaction

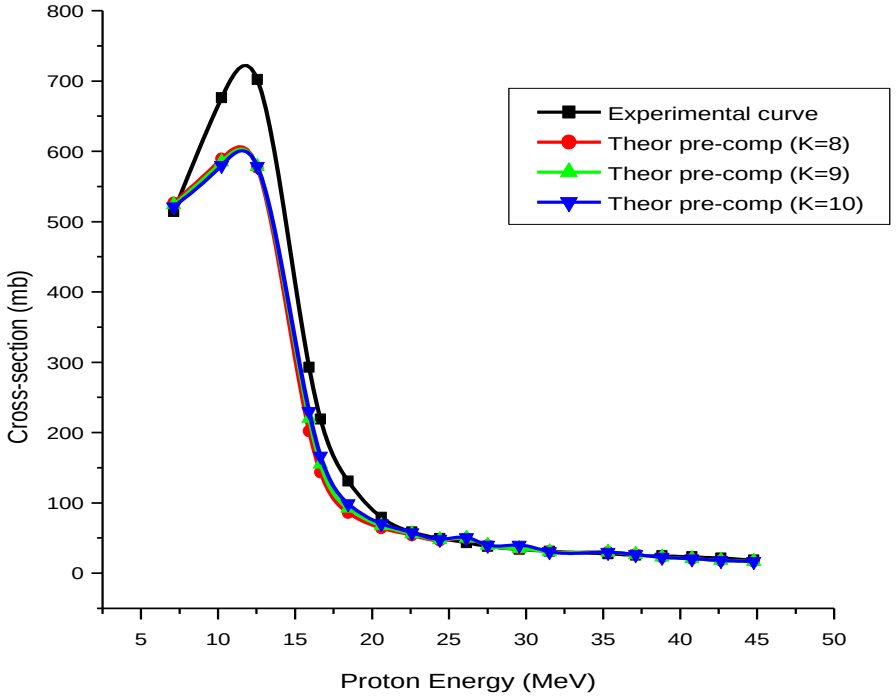

Figure 5.1: Comparing PLD values for pre-compound reaction of $^{51}V(p,n)$.

The change in level density parameter has negligible effect on the shape as well as the size of the excitation function of $^{51}V(p,n)^{51}Cr$ reaction as shown in Figure 5.1. The excitation function is slightly higher for smaller K values for proton energies up to about 13 MeV and between about 13 and 23 MeV, the excitation function is slightly higher for larger K values. In the proton energy above about 23 MeV, all excitation function curves overlap. A similar effect is seen on the theoretical equilibrium excitation function except in that all compound excitation functions fall to zero above around 25 MeV as shown in Figure 5.2. The value K = 9 is on the average preferable.

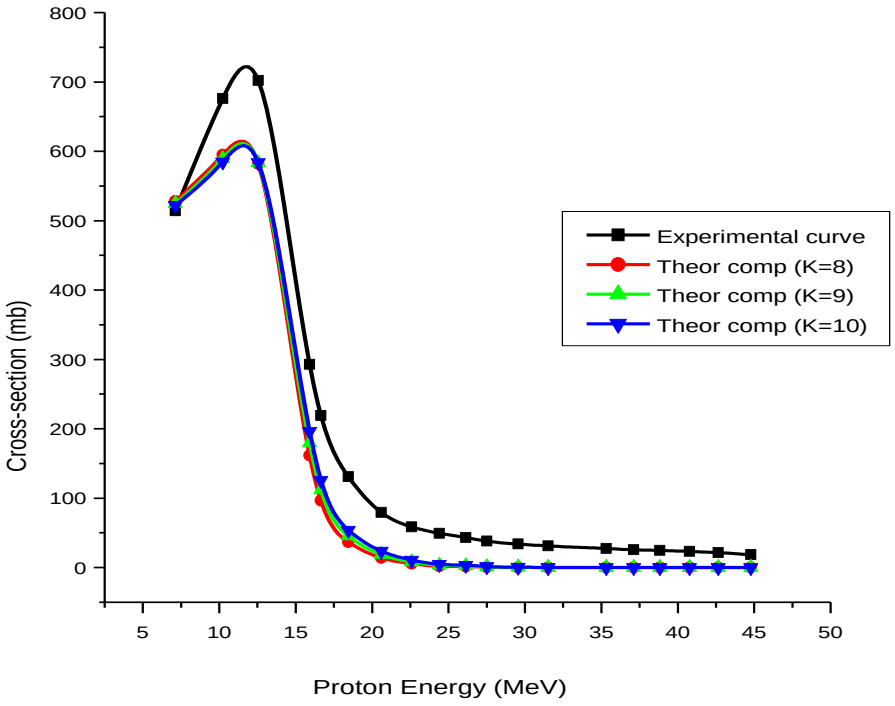

Figure 5.2: Comparing PLD for equilibrium decay of ^{51}V(p,n) .

B. $^{51}V(p,3n)$ and $^{51}V(p,4n)$ reactions

As we can see in Figure 5.3, the change in level density parameter has slight effect on the theoretical pre-compound reaction cross-section at proton energies above around 35 MeV. Above this energy, the pre-equilibrium excitation function is higher for larger K values. However, all theoretical excitation functions are not comparable to the experimental excitation function. The same effect is observed on the equilibrium excitation function.

Figure 5.4 shows that the change in level density parameters for ^{51}V(p,4n), has some visaible effect at proton energies above 50 MeV. The theoretical excitation function curve at higher energies is higher for larger values of K. However, all theoretical cross-section values are not comparable to the experimental cross-section values. The same effect is observed on its equilibrium excitation function.

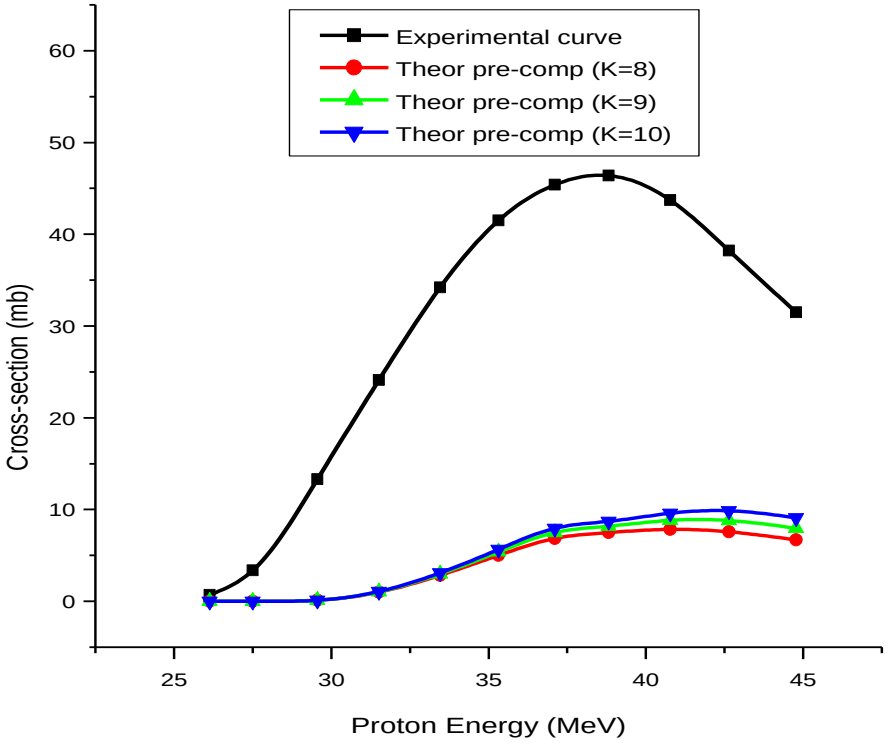

Figure 5.3: Effects of PLD on pre-compound excitation function of $^{51}V(p,3n)$

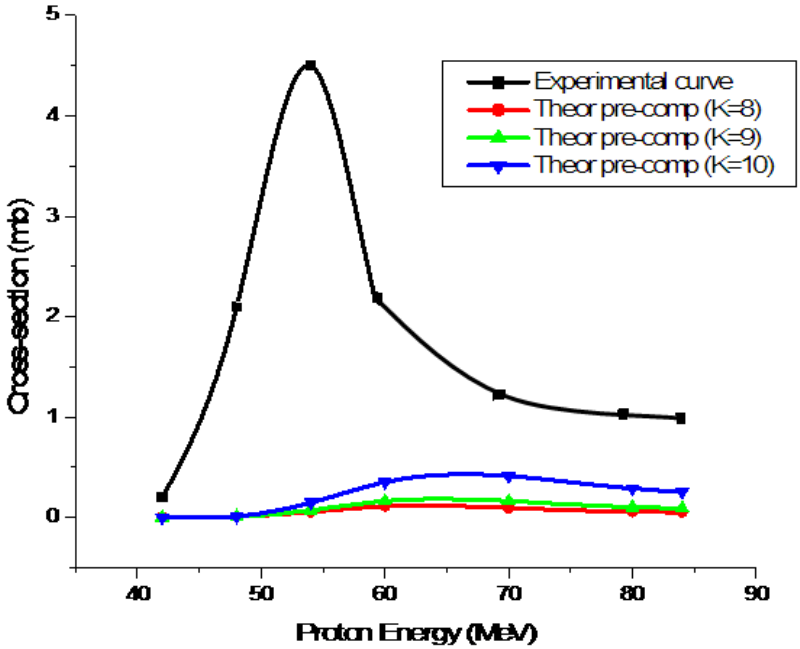

Figure 5.4: Effects of PLD on pre-compound cross-sections $^{51}V(p,4n)$.

C. $^{209}Bi(p,n)^{209}Po$ reaction

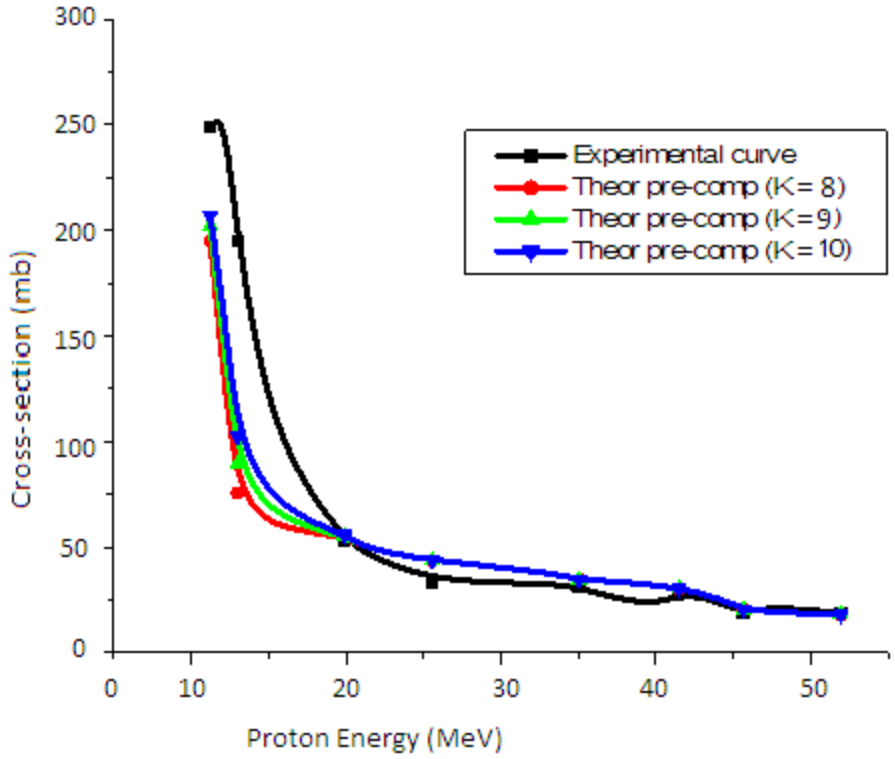

Figure 5.5: Effect of PLD on pre-equilibrium cross-sections of ^{209}Bi(p,n)

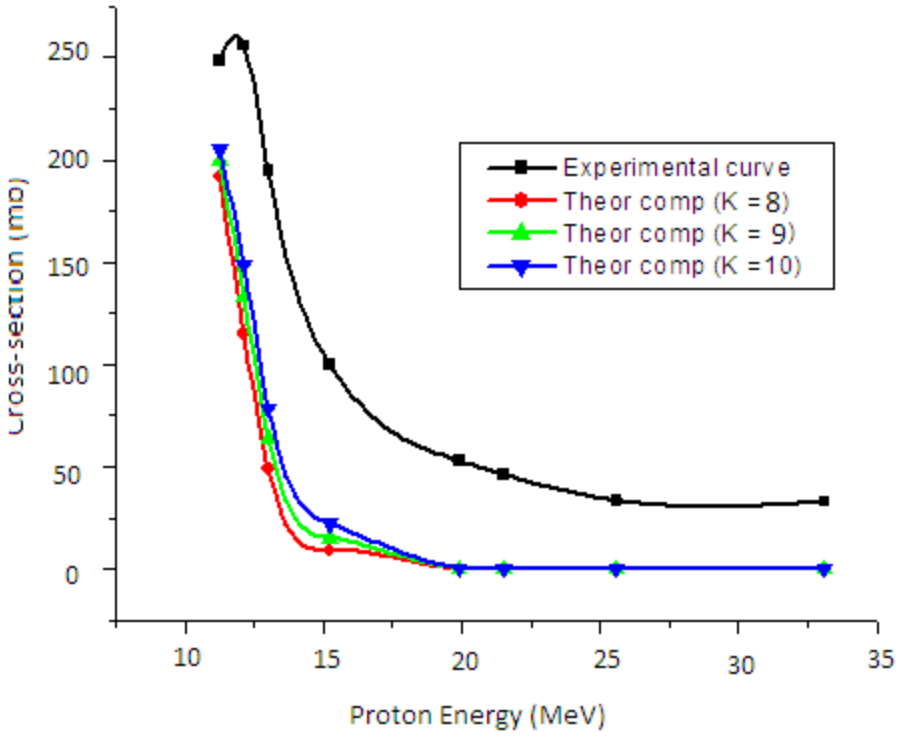

Figure 5.6: Effect of PLD on equilibrium excitation function of ^{209}Bi(p,n)

The change in PLD slightly affects the shape as well as the size of the pre-equilibrium excitation function of $^{209}Bi(p,n)^{209}Po$ reaction for proton energies less than about 25.58 MeV. In this region, the excitation function curve due to K = 10 is slightly closer to the experimental curve.

In the case of equilibrium excitation functions of this same reaction, the change in level density parameter slightly affects the shape as well as the size of the equilibrium excitation function curves for proton energies less than about 19.91 MeV as shown in Figure 5.6. Above this energy, cross-sections due to all values of K fall to zero. The excitation function curve due to K = 10 is relatively closer to the experimental curve than the other curves particularly at lower energies.

$^{209}Bi(p,3n)^{207}Po$ reaction

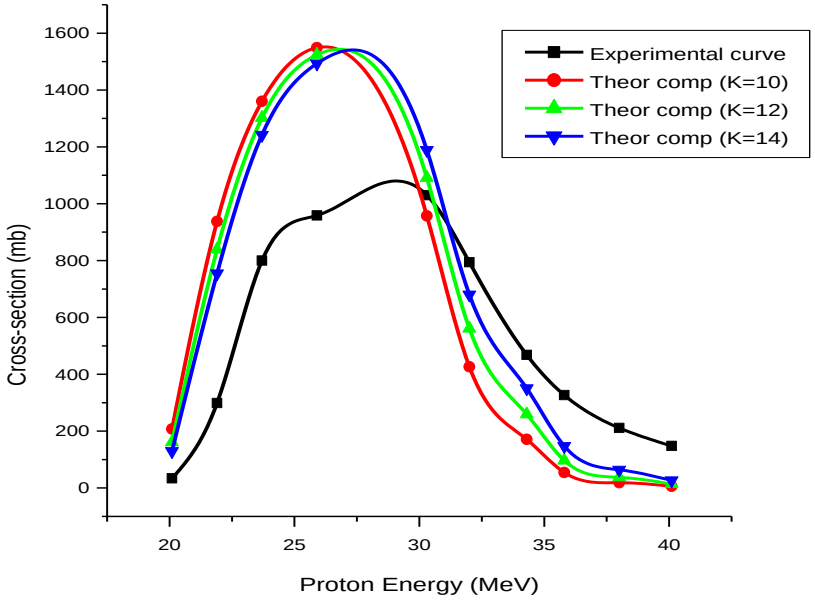

Figure 5.7: Effect of PLD on equilibrium excitation function of $^{209}Bi(p,3n)$.

As the parameter K increases, the theoretical equilibrium cross-section peaks of $^{209}Bi(p,3n)^{207}Po$ reaction shift towards the increasing energy as shown in Figure 5.7. As the value of K increases, the corresponding cross-section values decrease at lower energies and increase at higher energies. The theoretical cross-section values due to K = 14 is nearer to that of the experimental values.

D. $^{209}Bi(p,4n)$ reaction

Figure 5.8 compares the excitation function curve of $^{209}Bi(p,4n)^{206}Po$ reaction. It is clear that the theoretical pre-compound excitation function curve is nearer to the experimental curve at almost all proton energies in the given range for K = 14. As the parameter K increases, the theoretical equilibrium cross-section peaks of $^{209}Bi(p,4n)^{206}Po$ reaction shift towards the increasing energy. As the value of K increases, the cross-section values decrease at lower energies and increase at higher energies.

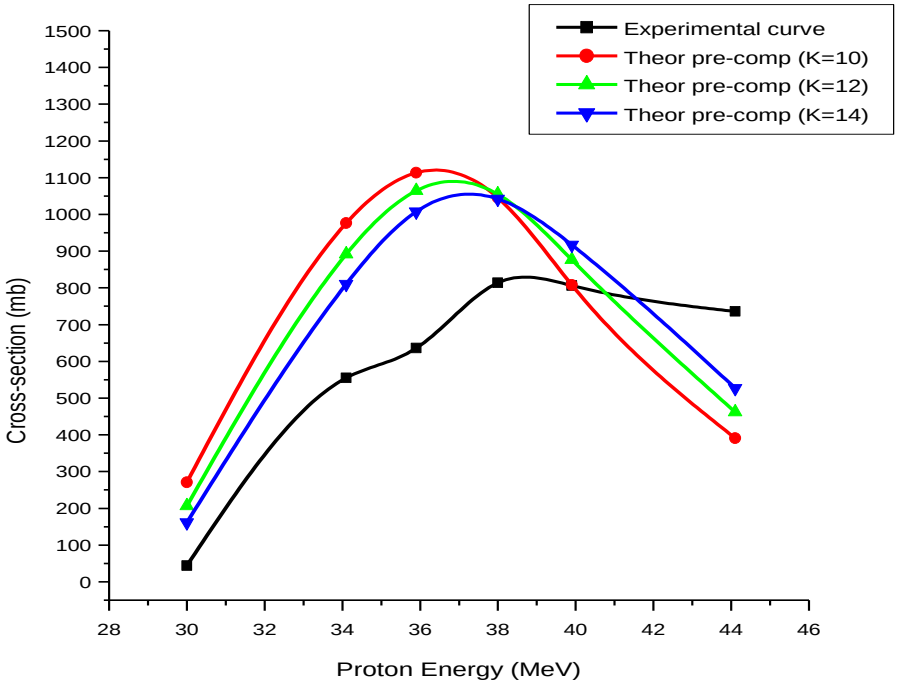

Figure 5.8: Effects of PLD on pre-equilibrium excitation function of $^{209}Bi(p,4n)$.

5.1.2. Effects of CMFP values on PE excitation functions

Effects of different CMFP values on pre-equilibrium excitation functions are compared using the initial exciton number $n_0 = 3(1p+1n+1h)$ and using appropriate level density parameters selected in the comparisons done in section 5.1.1.

A. $^{51}V(p,n)^{51}Cr$ and $^{51}V(p,3n)^{49}Cr$ reactions

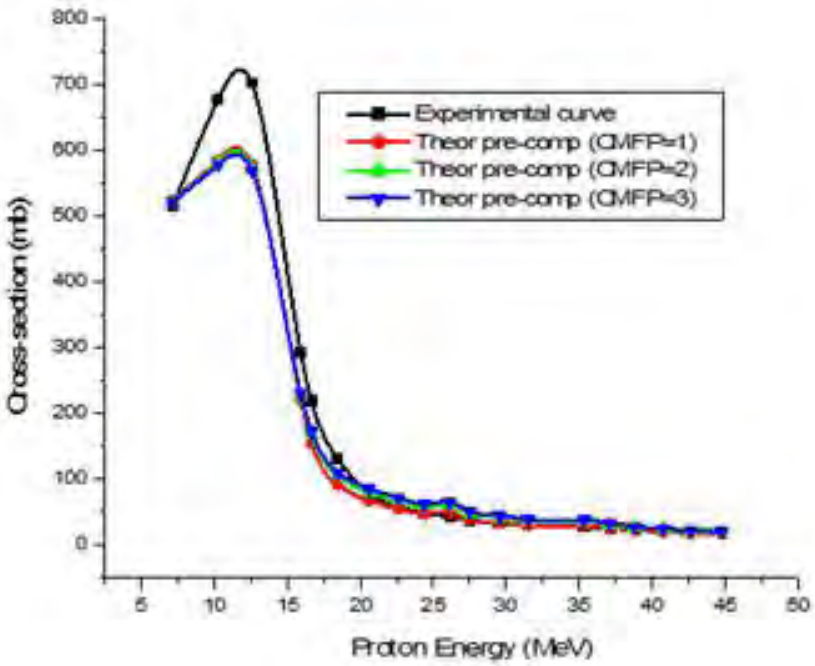

Figure 5.9: : Effect of CMFP values on excitation functions of $^{51}V(p,n)$ at a = $A_{CN}/9$.

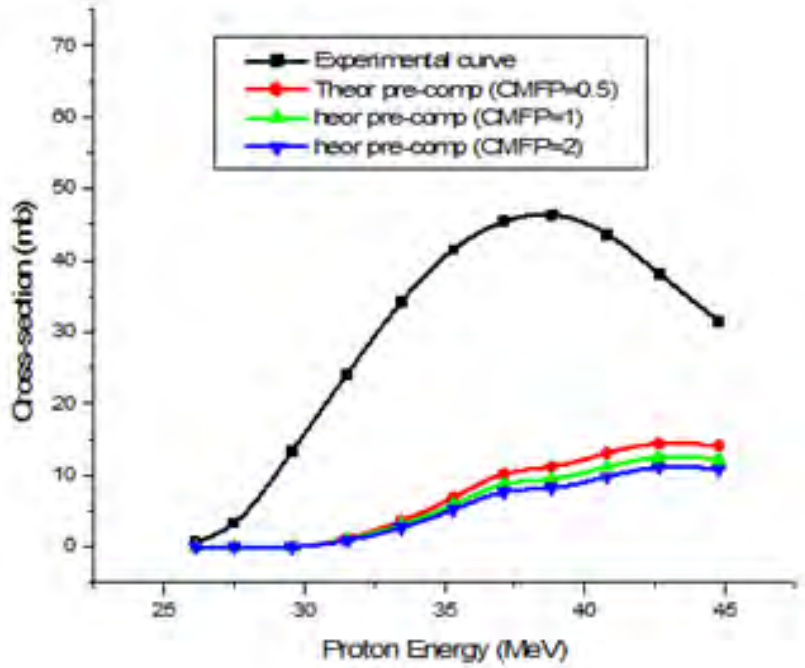

Figure 5.10: Effect of CMFP values on excitation functions of $^{51}V(p,3n)$ at a = $A_{CN}/10$

At lower energies (< 20 MeV), changing the CMFP value has no effect on the excitation function of ^{51}V(p,n) reaction and for energies above 20 MeV, the cross-section σ(p,n) is nearly zero. As we can see in Figure 5.9, the excitation function curve calculated by CMFP = 1.000 is slightly closer to the corresponding experimental curve.

The change in CMFP value for ^{51}V(p,3n) reaction slightly affects the theoretical cross-section values at projectile energies of about above 33 MeV as shown in Figure 5.10. We can see that the theoretical cross-section is higher for smaller CMFP values.

As we have discussed in section 5.1.1, all compound and pre-compound excitation functions for the reactions ^{51}V(p,3n) and ^{51}V(p,4n) are not comparable to the corresponding experimental excitation functions.

B. ^{209}Bi(p,n)^{209}Po reaction

Figure 5.11 shows that the CMFP values for the pre-compound reaction of ^{209}Bi(p,n) affects the shape as well as the size of the excitation functions appreciably at proton

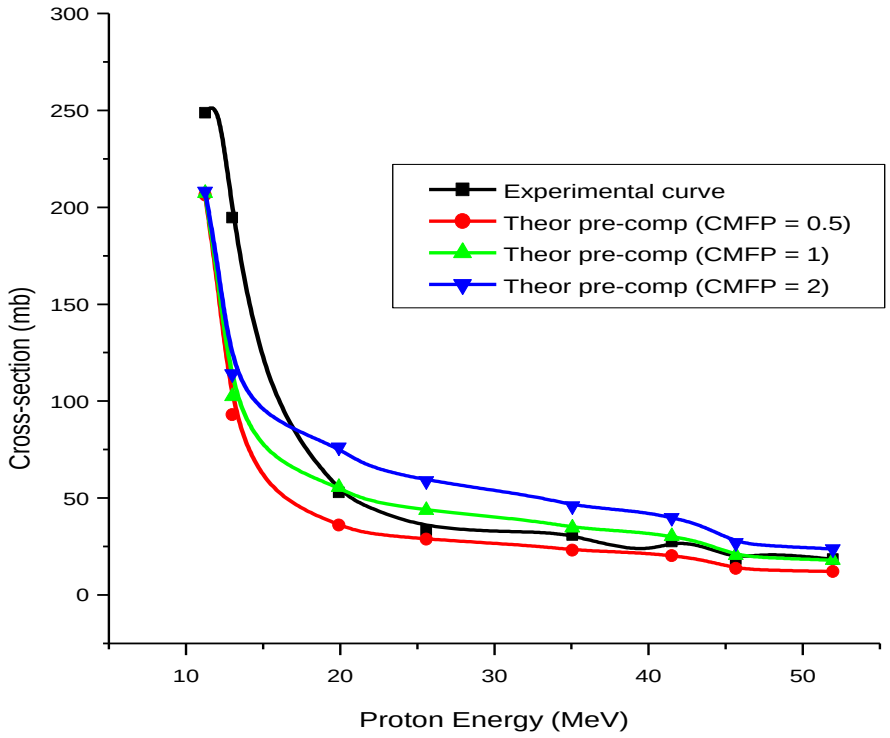

Figure 5.11: Comparing CMFP values for ^{209}Bi(p,n) reaction, a = A_{CN}/10

energies above about 13 MeV. We can see that above this energy, the excitation function due to CMFP = 1.000 best fits to the experimental curve.

C. $^{209}Bi(p,3n)^{207}Po$ reaction

The change in CMFP value has significant effect at all proton energies for $^{209}Bi(p,3n)^{207}Po$ reaction. CMFP = 3 is relatively suitable as seen in Figure 5.12.

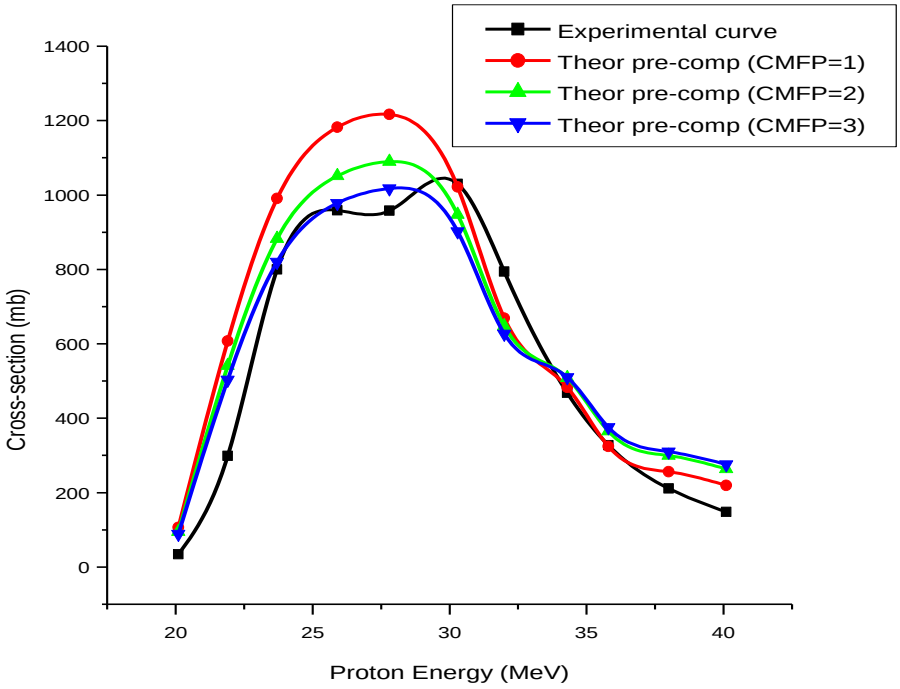

Figure 5.12: Comparing CMFP values for ^{209}Bi(p,3n) reaction , a = A_{CN}/14

D. $^{209}Bi(p,4n)^{206}Po$ reaction

Change in CMFP in $^{209}Bi(p,4n)^{206}Po$ reaction has significant effect on the excitation functions as shown in Figure 5.13. CMFP = 2 is used for the final reaction.

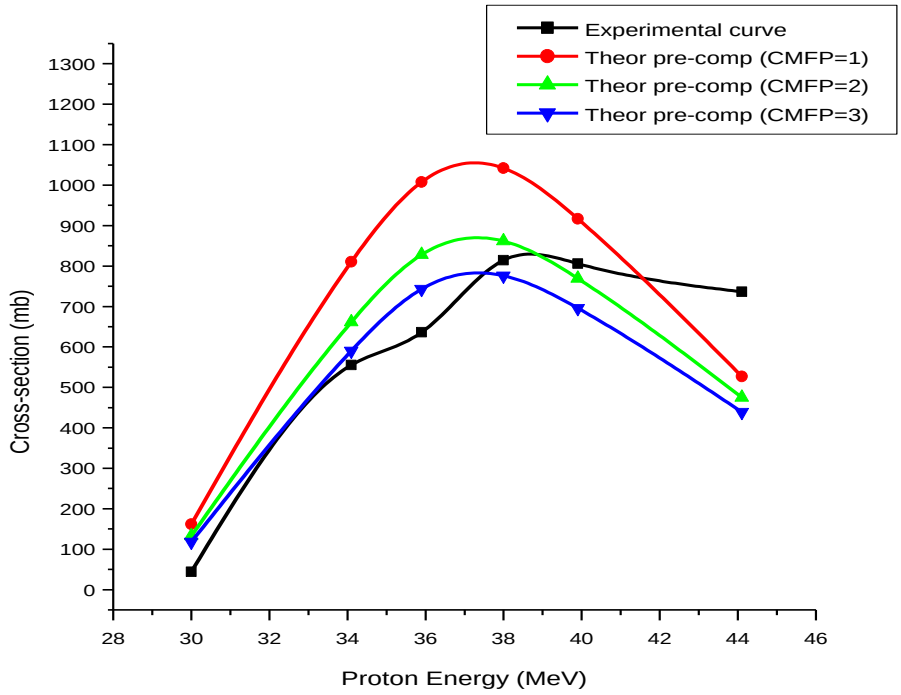

Figure 5.13: Comparing CMFP values for ^{209}Bi(p,4n) reaction, a = A_{CN}/14.

Observations on section 5.1

From the analyses in section 5.1, we observed that changes in CMFP and PLD values have no significant effects for proton energies below 20 MeV. This effect of the CMFP values confirm eqn. 2.22 in chapter 2 that the mean free path of a reaction depends on excitation energy above 20 MeV proton energy only, but constant below this energy. The result for PLD values also confirms implications of eqns. 2.23 and 2.24 in chapter 2. These equations, representing Fermi model and constant temperature model, imply that level density depends on PLD values only above the matching point, but does not depend on PLD values below the matching point.

5.2. Comparing calculated and measured cross-sections

In the analyses given in section 5.1, relatively appropriate input parameters are selected and these selected parameters are used in theoretical reaction cross-section calculations. In this section, theoretical and experimental results are compared using

graphs. The data tables include experimental data, uncertainties of the experimental data, theoretical equilibrium cross-section values, theoretical pre-equilibrium cross-section values and proton projectile kinetic energies. Input parameters used in theoretical calculations are also included at the last rows of the corresponding tables.

The size of the vertical line on each experimental curve (black line) represents the magnitude of the experimental uncertainty at that particular value. The equilibrium and the pre-equilibrium excitation function curves are traced with red and green lines, respectively. Cross-section values are measured in milli-barn (mb) and kinetic energies in mega-electronvolt (MeV).

5.2.1. Excitation functions of (p,n) reactions

Table 5.1: Theoretical and Experimental Cross-sections for $^{51}V(p,n)^{51}Cr$

$\varepsilon_p\,(MeV)$	$\sigma_{EX}\,(mb)$	$\sigma_{EQ}\,(mb)$	$\sigma_{PE}\,(mb)$	$\sigma_{ER-T}\,(mb)$
7.13	514	524.9	523.8	62
10.23	676	589.4	584.6	81
12.55	702	583.5	578.1	49
15.91	293	179.8	219.9	35
16.66	219	111.8	155.3	15
18.45	131	45.36	92.53	9
20.59	79.4	18.71	67.33	5.6
22.58	58.4	7.978	55.66	4.1
24.41	49.1	3.269	47.4	3.9
26.14	43.4	2.477	49.9	3.9
27.5	38.2	0.9821	39.62	6.1
29.56	33.9	0.4257	34.82	5.4
31.52	31.3	0.184	30.49	5
35.32	27.4	0	29.96	4.3
37.11	25.8	0	26.35	4.1
38.82	24.8	0	22.79	4

Input parameters used: n_0 = 3(1p+1n+1h), a = ACN//9, CMFP = 1

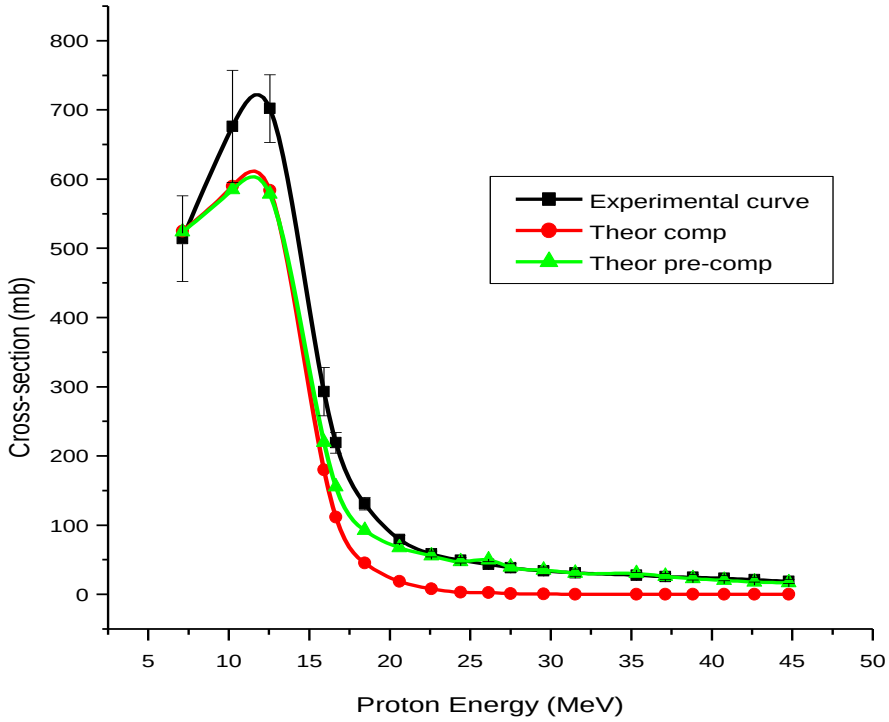

Figure 5.14: Experimental and theoretical excitation functions for $^{51}V(p,n)$

Table 5.2: Theoretical and Experimental Cross-sections for $^{209}Bi(p,n)^{209}Po$

ε_p (MeV)	σ_{EX} (mb)	σ_{EQ} (mb)	σ_{PE} (mb)	σ_{ER-T} (mb)
11.24	248.7	205.3	207.2	27.59
12.13	256.1	148.7	160.8	35.01
13.01	194.7	78.66	102.4	23.29
15.22	99.99	22.12	69.84	13.67
19.91	52.88	0.4821	55.61	7.912
21.51	46.11	0.091	48.65	6.901
25.58	33.37	0	43.61	4.959
33.1	32.72	0	37.94	4.472
35.05	30.85	0	34.57	3.955
39.47	21.47	0	32.49	3.175
41.51	27.43	0	30.18	2.56
43.37	25.86	0	27.53	2.643
45.67	18.53	0	20.35	2.69
47.61	21.89	0	19.13	2.619
51.95	18.53	0	17.9	2.056

Input parameters used: n_0 = 3(1p+1n+1h), ACN/14, CMFP= 1

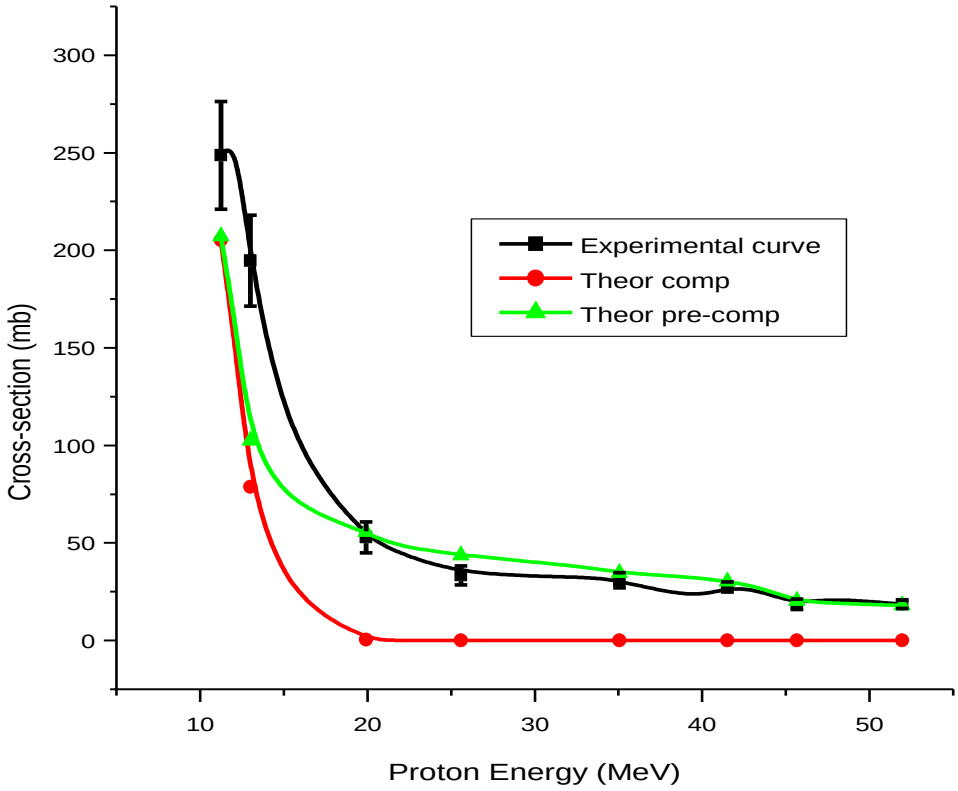

Figure 5.15: Experimental and theoretical excitation functions for ^{209}Bi(p,n).

In $^{51}V(p,n)^{51}Cr$ reaction, both the theoretical compound and the theoretical pre-compound excitation functions are comparable with the experimental excitation function up to about 17 MeV. Above this energy, the excitation function curve in the equilibrium emission lowers rapidly and eventually comes to zero at proton energies above around 20 MeV as shown in Figure 5.14.

Similarly, for $^{209}Bi(p,n)^{209}Po$ reaction shown in Figure 5.15, both the theoretical equilibrium and the theoretical pre-equilibrium excitation functions were comparable to the experimental excitation function up to around 13 MeV. Above this energy, the equilibrium excitation function curve falls to zero rapidly. In the two reactions, the long tails in the experimental results at higher proton energies are explained properly on the basis of pre-compound theory only.

Observations on (p,n) reactions

From excitation functions of ^{51}V(p,n) and ^{209}Bi(p,n) reactions in Figure 5.16, we can see that cross-section peaks in the two reactions occur at almost the same proton energies - around between 11 to 12 MeV. However, the theoretical and experimental cross-section peaks of ^{51}V(p,n) are about 2.7 fold higher than that of ^{209}Bi(p,n) reaction. This shows that the p+V has the greatest probability to occur than that of p+Bi reaction in the corresponding energy range. This result confirms eqn. 2.27 in chapter 2 that for processes involving evaporation in p+V and p+Bi reactions, the cross-section of the first is greater than that of the second for proton energies below around 21 MeV. From the above expressions, we can also see that the threshold energy for V(p,n) is less than that of Bi(p,n) reaction; but the excitation function curve of the later falls more rapidly than that of the first. That is, the energy range for p+V is greater than that of p+Bi reaction.

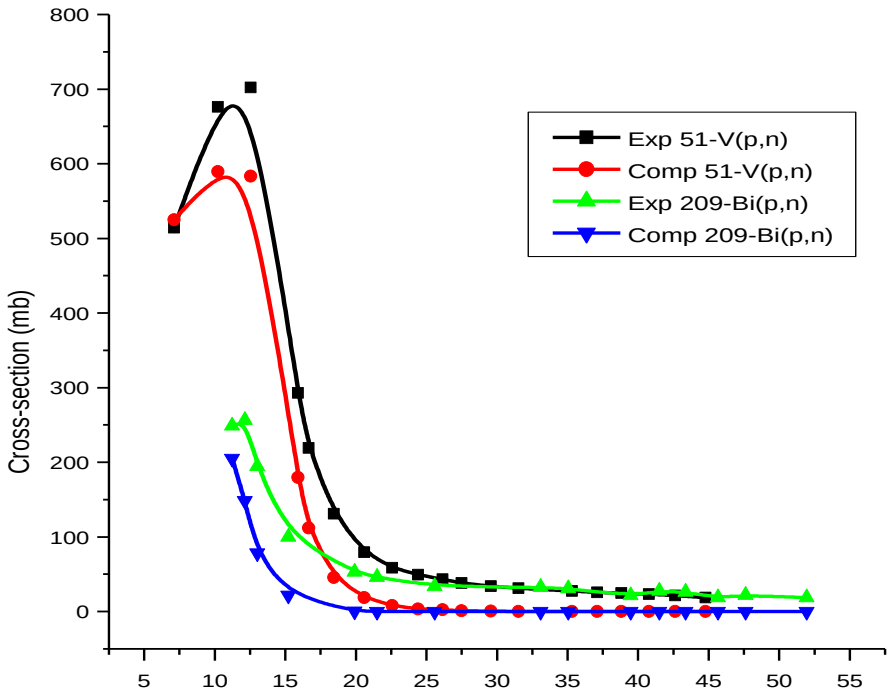

Figure 5.16: Measured and calculated excitation functions for ^{51}V(p,n) and ^{209}Bi(p,n).

5.2.2. Comparison on excitation functions of (p,3n) reactions

Table 5.3: Theoretical and Experimental cross-sections for $^{51}V(p,3n)^{49}Cr$

ε_p (MeV)	σ_{EX} (mb)	σ_{EQ} (mb)	σ_{PE} (mb)	σ_{ER-T} (mb)
26.14	0.68	0	0	0.21
27.5	3.35	0	0	0.47
29.56	13.3	0.1702	0.1032	1.7
31.52	24.1	1.814	1.068	2.8
33.46	34.2	5.361	3.11	3.8
35.32	41.5	9.851	5.664	4.9
37.11	45.4	14	7.962	5.1
38.82	46.4	15.67	8.728	5.1
40.77	43.7	16.94	9.612	4.8
42.64	38.2	16.42	9.863	4.2
44.78	31.5	14.47	9.083	3.5

Input parameters used: n_0 = 3(1p+1n+1h), ACN/10, CMFP = 0.5

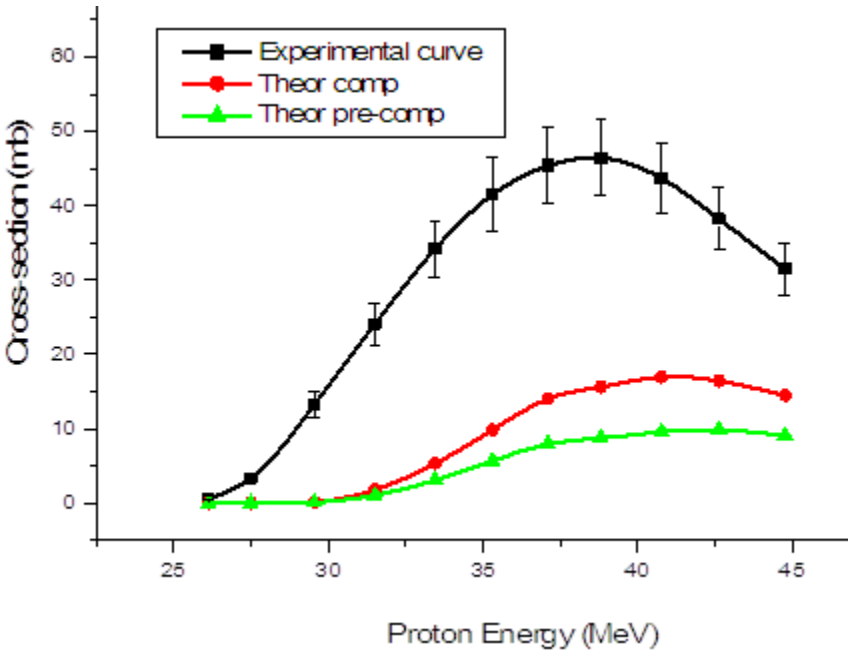

Figure 5.17: Experimental and Theoretical excitation functions for $^{51}V(p,3n)$ reaction.

Table 5.4: Theoretical and Measured cross-sections for $^{209}Bi(p,3n)^{207}Po$

ε_p (MeV)	σ_{EX} (mb)	σ_{EQ} (mb)	σ_{PE} (mb)	σ_{ER-T} (mb)
20.1	33.9	106.5	73.48	
21.9	299	682	457.4	27
23.7	800	1182	783.1	75
25.9	959	1457	954.9	92
30.3	1030	1262	932.3	97
32	794	783.7	672.2	79
34.3	468	439.5	483.2	47
35.8	327	203.7	324.1	31
38	211	96.03	255.8	19
40.1	148	43.54	189.4	15
Input parameters used: a = A_{CN}/14.00, CMFP = 3.00				

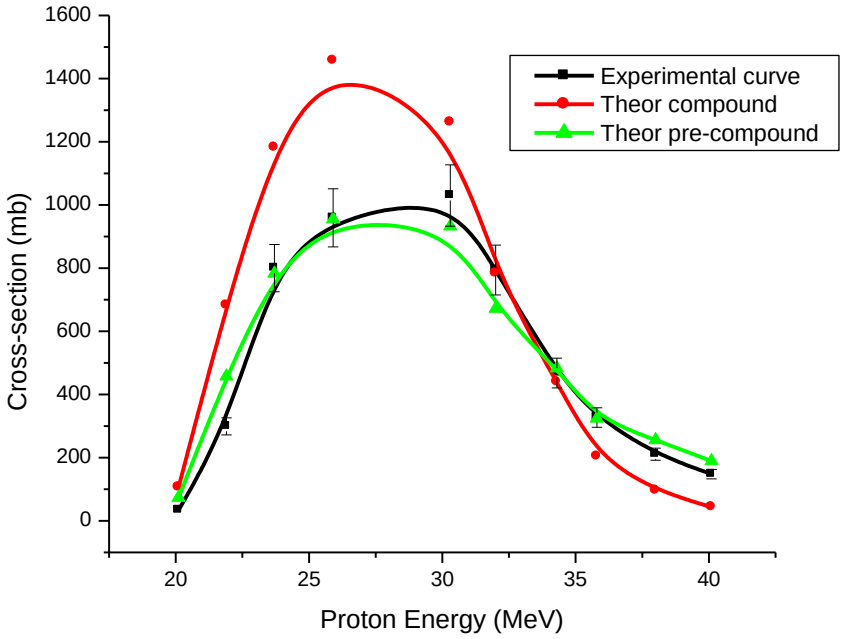

Figure 5.18: Measured and calculated excitation functions for $^{209}Bi(p,3n)$.

Both the theoretical compound and the theoretical pre-compound excitation functions of the $^{51}V(p,3n)^{49}Cr$ reaction are not comparable with the corresponding experimental excitation function in the given proton energy range as shown in Figure 5.17. The experimental cross-section peak is about 2.7 fold greater than that of the theoretical cross-section peaks. This very high experimental excitation function curve compared to

the theoretical excitation function curves indicates that the reaction may take place by direct reaction.

In the case of ^{209}Bi(p,3n) reaction shown in Figure 5.18, the theoretical pre-compound excitation function is more comparable to the experimental excitation function at most energies than that of the equilibrium excitation function. The equilibrium excitation function is more comparable to the experimental excitation function than that of the pre-equilibrium excitation function at around 32 MeV proton energies. At higher energies, the compound cross-section values fall towards zero but the pre-compound cross-section values remain above the experimental values.

Observations on (p,3n) reactions

As we can see in Figure 5.17 and Figure 5.18, the cross-section peak of the ^{209}Bi(p,3n) reaction occurs at around 30 MeV whereas that of the ^{51}V(p,3n) reaction occurs at around 40 MeV proton energies. Higher projectile energy for a lighter target may confirm that the reaction takes place by direct reaction mechanism (see eqn. 2.21).

5.2.3. Excitation functions of (p,4n) reactions

Table 5.5: Theoretical and Experimental cross-sections for $^{51}V(p,4n)^{48}Cr$

ε_p (MeV)	σ_{EX} (mb)	σ_{EQ} (mb)	σ_{PE} (mb)	σ_{ER-T} (mb)
42	0.2	0	0	
48	2.1	0.01169	0.00978	
54	4.5	0.1363	0.05625	
60	1.8	0.2595	0.1129	
70	1.7	0.1623	0.09417	
80	1.1	0.04775	0.05702	

Input parameters used: n_0 = 3(1p+1n+1h), ACN/10, CMFP= 3

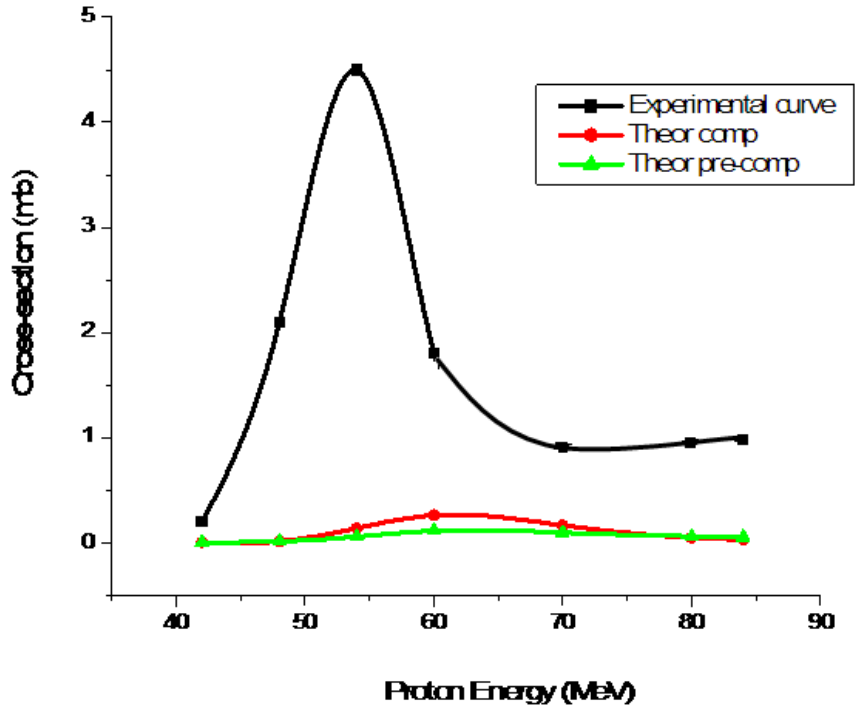

Figure 5.19: Experimental and Theoretical excitation functions for $^{51}V(p,4n)$.

Table 5.6: Theoretical and Measured cross-sections for $^{209}Bi(p,4n)^{206}Po$ reaction

ε_p (MeV)	σ_{EX} (mb)	σ_{EQ} (mb)	σ_{PE} (mb)	σ_{ER-T} (mb)
30	44.2	238.6	132.3	
34.1	555	1242	661.2	49
35.9	636	1538	828	56
38	814	1552	861.4	76
39.9	806	1102	769.3	80
44.1	736	588.6	475	72
Input parameters used: n_0 = 3(1p+1n+1h), ACN/14, CMFP = 2				

Both compound and pre-compound excitation functions of $^{51}V(p,4n)$ are appreciably lower than that of the corresponding experimental ones as shown in Figure 5.20. Higher experimental curve compared to the theoretical curves indicates that neither compound nor pre-compound decay occurs but the reaction may take place by direct reaction.

In the case of $^{209}Bi(p,4n)$ reaction, only pre-compound theory describes the experimental cross-section values only up to about 42 MeV proton energies; and higher

experimental curve above 42 MeV indicates that at higher energies the reaction may take place by direct reaction.

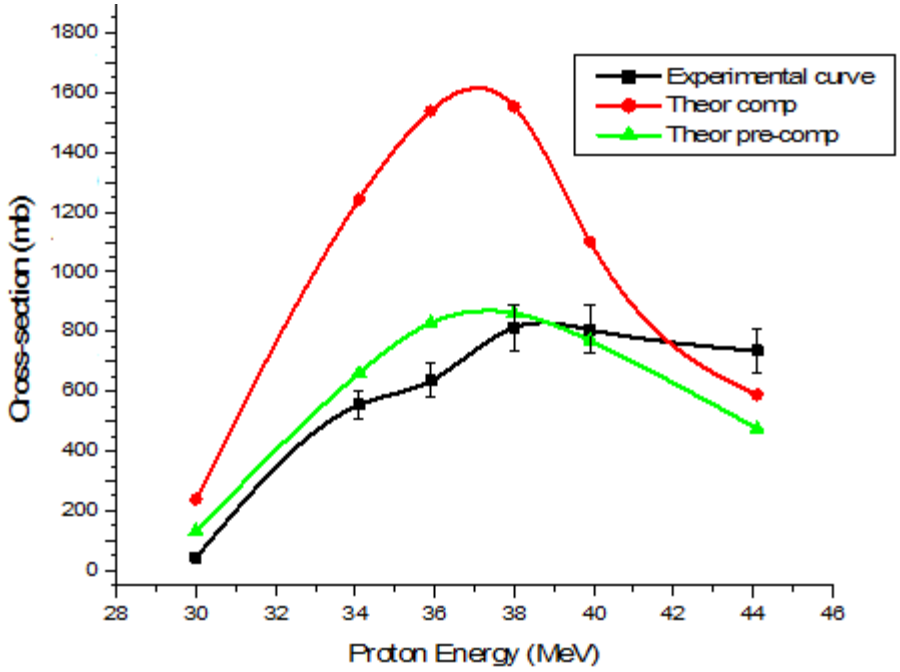

Figure 5.20: Experimental and Theoretical excitation functions for ^{209}Bi(p,4n).

5.2.4. Confirmation of absence of EQ decay in some reactions

For processes involving evaporation, the cross-section peak increases with increasing energy. It can be seen in Figure 5.21 and Figure 5.22 that this theory fails for ^{51}V(p,3n), ^{51}V(p,4n) and ^{209}Bi(p,4n) reactions. This shows that no equilibrium decay take place in these reactions.

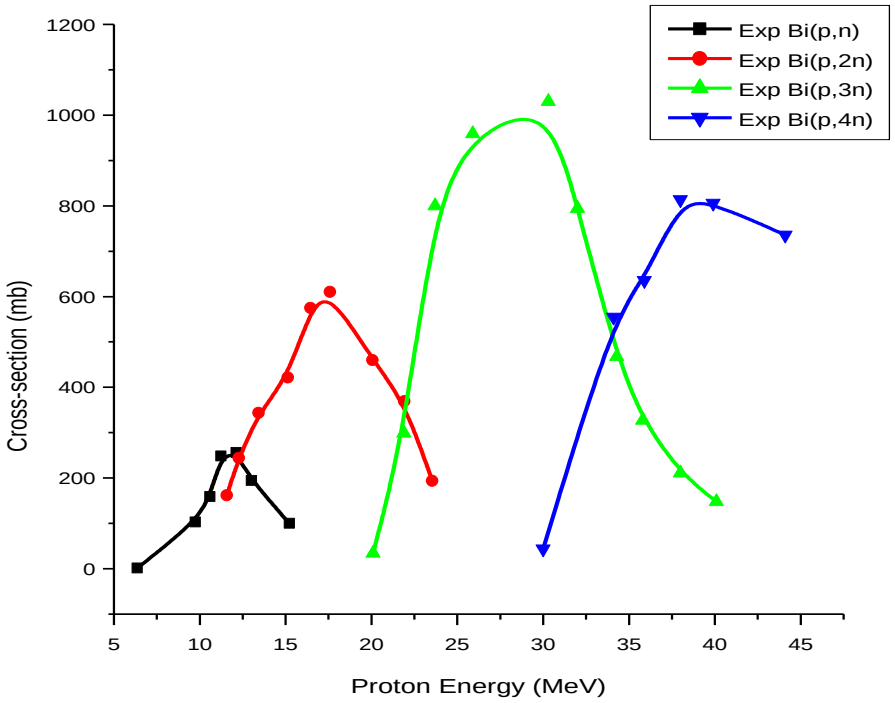

Figure 5.21: Peak cross-section variation with proton energy for ^{209}Bi(p,xn) reactions.

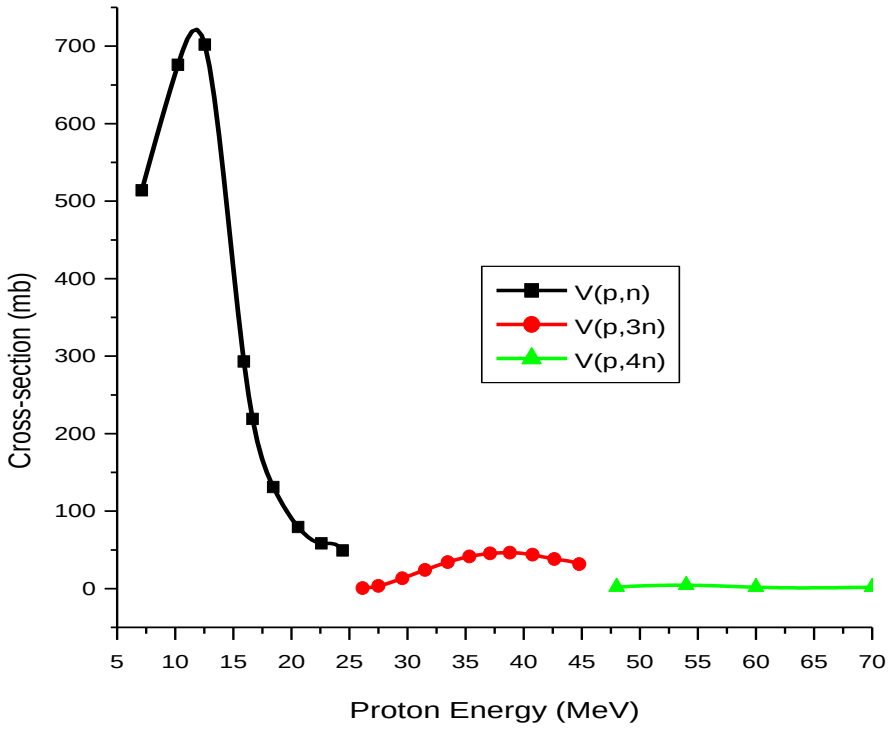

Figure 5.22: Peak cross-section variation with proton energy for ^{51}V(p,xn) reactions.

5.3. Conclusion

From the present study of excitation functions, the pre-compound theory works in the given proton energy range for $^{51}V(p,n)^{51}Cr$, $^{209}Bi(p,n)^{209}Po$, and $^{209}Bi(p,3n)^{207}Po$ reactions shown in Figure 5.14, Figure 5.15 and Figure 5.18, respectively, and below around 40 MeV for $^{209}Bi(p,4n)^{206}Po$ reaction shown in Figure 5.20. However, the compound nucleus theory works at proton energies below 20 MeV for the first two reactions and at a small energy range between 30 and 35 MeV for the third reaction only. The long tails of the experimental excitation functions at higher energies in the first three reactions are described by pre-equilibrium reaction excitation functions only. However, the pure equilibrium reaction in its decay is unable to explain the experimental data especially in the high energy tail portion of the excitation functions.

Very high experimental excitation functions of $^{51}V(p,3n)$ and $^{51}V(p,4n)$ reactions compared to both theoretical compound and pre-compound excitation functions in the corresponding energy ranges as shown in Figure 5.17 and Figure 5.19, indicate that these reactions may undergo by direct reaction. Similarly, the very high experimental excitation function of $^{209}Bi(p,4n)$ compared to both theoretical compound and pre-compound excitation functions above 40 MeV proton energies indicate that the reaction above this energy may be direct reaction. Generally, our analyses which show that compound nucleus decay takes place only at lower energies for the target of lighter nuclei (^{51}V) and at lower and medium energies for the target of heavier nuclei (^{209}Bi), agree with Bohr's second hypothesis.

Figure 5.16 shows that the cross-section (both experimental and theoretical) of $^{51}V(p,n)$ reaction is greater than that of $^{209}Bi(p,n)$ reaction. Higher cross-section of the smaller target compared to that of the heavier target for proton energies below about 20 MeV agrees with our calculated value of eqn. 2.27 in chapter 2. This result shows that there is greater probability for the reaction to take place for $^{51}V(p,n)$ than that of $^{209}Bi(p,n)$.

We can see from the analysis in section 5.1, that changes in CMFP and PLD values have no visible effects on excitation functions in proton energies below around 20 MeV, but have some effects above this energy. This result for CMFP values also agree with the description in chapter 2 that the mean free path depends on excitation energy above 20 MEV proton energies.

References

[1] N. Bohr, Nature, 137, 344 (1936).

[2] V.F. Weisskopf, Problems of nuclear Structure, Phys. Today, July 1961, 18.

[3] S.N. Goshal; Atomic and Nuclear Physics Vol-II, S.chand and company Ltd; New Delhi (1997)

[4] E. Gadioli and P.E. Hodgson, Pre-equilibrium nuclear reactions, Oxford Univ. Press 1992

[5] K.chen, G.Friedlander, G.D.Harp and J.M.Miller:Phys.Rev.166(1966)949.

[6] A.J. Koning and J.M. Akkermans, Ann. Phys. (N.Y.), 208, no.1 (1991), 216.

[7] J.J. Griffin, Phys. Rev. Left. 17 (1966), 478.

[8] C.K. Cline and M. Blann, Nucl. Phys. A172 (1971), 225.

[9] W.D.Myres and W.J Swiatecki.Nucl.Phys 81(1966)01: ArkFys.36 (1967)343.

[10] M.K. Bhardwaj, I.A.Rizivi, and A.K. Chaubey, Phys.Revs.C Vol45, 2338-2342(1992)

[11] EXFOR IAEA,Vienna, 2004.

[12] G.R. Satchler, Direct Nuclear Reactions, Oxford University Press (New York, 1983).

[13] Multistep Direct Reactions, Faure, South Africa, ed. R.H. Lemmer, World Scientific (1992).

[14] Measurement and Hybrid-Model Analysis of Proton-Induced Reactions with V,Fe, and Co. (R.Michel,G.Brinkmann,H.Weigel,W.Herr)

[15] The cross section and the recoil range study of the ^{209}Bi(p,n) and (p,2n) reactions, (K.Miyano, H.Nakahara)

[16] (P,XN) Reactions Induced in Tm-169, Ta-181 and Bi-209 With 20 to 45 MeV Protons, (C.BIRATTARI, E.GADIOLI, A.M.GRASSI STRINI, G.STRINI, G.TAGLIAFERRI, L.ZETTA)

[17] Interaction of vanadium with protons of energies up to 84 MeV, (S.Hontzeas,L.Yaffe)

[18] 1999 - FH Combley, 2005 - CN Booth, 2009 - NJC Spooner

[19] W.D. Ehmann and D.E. Vance, Radiochemistry-and-Nuclear-Methods-of-Analysis- (Wiley, New York, 1991).